

1 Dear Editor,
2 Please find below the version of the manuscript with tracked changes. I made all the requested
3 corrections:

- 4 - Reorganisation of the paragraph page 11
- 5 - I changed the title of Section 6
- 6 - I reduced the conclusion
- 7 - Change all the “lower/upper tropospheric ozone” occurrence with “lower-/upper-
8 tropospheric ozone”

9 Thanks for considering this corrected version for publication.

10 Sincerely,

11 Gaëlle Dufour

12

13

14

15 **Springtime daily variations of lower tropospheric ozone**
16 **over East Asia: role of cyclonic activity and pollution as**
17 **observed from space with IASI**

Gaëlle Dufour 15/9/y 13:55

Supprimé:

18

19 **G. Dufour¹, M. Eremenko¹, J. Cuesta¹, C. Doche², G. Foret¹, M. Beekmann¹, A.**
20 **Cheiney^{3,1}, Y. Wang⁴, Z. Cai⁴, Y. Liu⁴, M. Takigawa⁵, Y. Kanaya⁵, and J.-M. Flaud¹**

21 [1] {Laboratoire Inter-universitaire des Systèmes Atmosphériques (LISA), UMR7583,
22 Universités Paris-Est Créteil et Paris Diderot, CNRS, Créteil, France}

23 [2] {Météo France, Direction Inter-Régionale Sud-Ouest, Division Etudes et Climatologie,
24 Mérignac, France}

25 [3] {Institut National de l'Environnement industriel et des RISques, INERIS, Verneuil-en-
26 Halatte, France}

1 [4] {Key Laboratory of Middle Atmosphere and Global Environment Observation, Institute of
2 Atmospheric Physics, Chinese Academy of Sciences, Beijing, China}

3 [5] {Japan Agency for Marine-Earth Science and Technology, Yokohama, Japan}

4 Correspondence to: G. Dufour (gaelle.dufour@lisa.u-pec.fr)

5

6 **Abstract**

7 We use satellite observations from IASI (Infrared Atmospheric Sounding Interferometer) on
8 board the MetOp-A satellite to evaluate the springtime daily variations in lower-tropospheric
9 ozone over East Asia. The availability of semi-independent columns of ozone from the
10 surface up to 12 km simultaneously with CO columns provides a powerful observational
11 dataset to diagnose the processes controlling tropospheric ozone enhancement at synoptic
12 scales. By combining IASI observations with meteorological reanalyses from ERA-Interim,
13 we elaborate an analysis method based only on IASI ozone and CO observations to identify
14 the respective roles of the stratospheric source and the photochemical source on ozone
15 distribution and variations over East Asia. The succession of low- and high-pressure systems
16 drives the day-to-day variations in lower-tropospheric ozone. A case study analysis of one
17 frontal system and one cut-off low system in May 2008 shows that reversible subsiding and
18 ascending ozone transfers in the upper troposphere lower stratosphere (UTLS) region due to
19 the tropopause perturbations occurring in the vicinity of low-pressure systems impact free and
20 lower-tropospheric ozone over large regions, especially north of 40°N, and largely explain the
21 ozone enhancement observed with IASI for these latitudes. Irreversible stratosphere-
22 troposphere exchanges of ozone-rich air masses occur more locally in the southern and south-
23 eastern flanks of the trough. The contribution to the lower-tropospheric ozone column is
24 difficult to dissociate from the tropopause perturbations generated by weather systems. For
25 regions south of 40°N, a significant correlation has been found between lower-tropospheric
26 ozone and carbon monoxide (CO) observations from IASI, especially over the North China
27 Plain (NCP). Considering carbon monoxide observations as a pollutant tracer, the O₃-CO
28 correlation indicates that the photochemical production of ozone from primary pollutants
29 emitted over such large polluted regions significantly contributes to the ozone enhancements
30 observed in the lower troposphere via IASI. When low-pressure systems circulate over the
31 NCP, stratospheric and pollution sources play a concomitant role in the ozone enhancement.
32 IASI's 3D observational capability allows the areas in which each source dominates to be

Gaëlle Dufour 15/9/y 13:55

Supprimé:

Gaëlle Dufour 15/9/y 13:55

Supprimé:

Gaëlle Dufour 15/9/y 13:56

Supprimé:

Gaëlle Dufour 15/9/y 13:56

Supprimé:

Gaëlle Dufour 15/9/y 13:56

Supprimé:

1 determined. Moreover, the studied cut-off low system has enough potential convective
2 capacity to uplift pollutants (ozone and CO) and to transport them to Japan. The increase of
3 the enhancement ratio of ozone to CO from 0.16 on 12 May over the North China Plain to
4 0.28 over the Sea of Japan on 14 May indicates photochemical processing during the plume
5 transport.

6

7 **1 Introduction**

8 In addition to being an important greenhouse gas (Stevenson et al., 2013), tropospheric ozone
9 (O_3) plays a central role in atmospheric chemistry and air quality, by controlling the oxidation
10 processes through the formation of hydroxyl radicals (OH) (Monks, 2005; Monks et al.,
11 2014). Ozone at high concentrations near the surface is a pernicious pollutant, harmful both to
12 human health and to vegetation (Seinfeld and Pandis, 1997, World Health Organization,
13 2013). Enhancements of ozone in the mid and lower troposphere result from photochemical
14 production from precursors (NO_x and hydrocarbons) and from stratosphere-troposphere
15 exchanges (STE) (Lelieveld and Dentener, 2000). The relative contributions made by these
16 sources depend on the season. It is well established that the peak activity of STE occurs
17 during winter and spring (Monks, 2000) whereas photochemical production is more active
18 during the summer period. The crucial role played by weather systems (cyclonic activity) in
19 determining tropospheric ozone variation has also been well established (e.g. Carmichael et
20 al., 1998; Cooper et al., 1998; Cooper et al., 2002a; Ding et al., 2009). These weather systems
21 are associated with tropopause perturbation, especially low tropopauses, and then with
22 subsiding and ascending ozone transfer in the upper troposphere – lower stratosphere (UTLS)
23 region. In addition, irreversible transfers of ozone can be expected, such as stratosphere-
24 troposphere exchanges that would take place preferentially on the western and southern flanks
25 of the trough (e.g. Ancellet et al., 1994; Holton et al., 1995; Liu et al., 2013), and downward
26 transport from the UTLS to the lower troposphere (e.g. Cooper et al., 2002a). Conceptual
27 models have been proposed to describe airstreams related to traveling low-pressure systems at
28 the midlatitudes (e.g. Cooper et al., 2002b). Two main mechanisms are responsible for part of
29 the ozone temporal and spatial variations observed in the troposphere. The dry airstream (DA)
30 occurring behind cold fronts is responsible for a strong downward transport of ozone from the
31 ULTS down to the middle troposphere. It is often linked to tropopause folding. This
32 downward transport can affect ozone concentrations down to the surface, especially at high

1 altitude sites (e.g. Carmichael et al., 1998; Schuepbach et al., 1999; Dempsey, 2014). In
2 contrast, air masses and then pollutants can be uplifted from the surface to the free
3 troposphere by different processes such as deep convection, orographic lifting and frontal
4 lifting (e.g. Bethan et al., 1998; Hannan et al., 2003; Miyazaki et al., 2003; Cooper et al.,
5 2004, Ding et al., 2009; Foret et al., 2014; Ding et al., 2015, and references therein). One part
6 of these processes, the warm conveyor belts (WCBs) associated with frontal activity and
7 lifting have been studied mainly in the scope of their role in the long-range transport of
8 pollutants, because they lift pollutants to levels where horizontal transport is more efficient.
9 Several studies focusing on the trans-Pacific transport of pollutants from East Asia towards
10 the United States have shown the importance of the frontal systems in this transport process
11 during springtime using both model simulations (e.g. Bey et al., 2001; Liu et al., 2003; Mari
12 et al., 2004; Lin et al., 2010) and dedicated field campaigns (e.g. Jaffe et al., 1999; Cooper et
13 al., 2004; Liang et al., 2004; Oshima et al., 2004). Very recently, Ding et al. (2015) have
14 shown that the topography of East Asia, as well as inducing orographic lifting, assists frontal
15 lifting and facilitates convection, thereby amplifying the possibility of pollutant uplifting.

16 In recent decades, East Asia and in particular China has experienced rapid economic growth.
17 The related increasing anthropogenic emissions of pollutants (Richter et al., 2005; Lin et al.,
18 2013) lead to regional ozone concentrations amongst the highest in the world (e.g. Chan and
19 Yao, 2008; Zhao et al., 2009; Lelieveld and Dentener, 2000; Wang et al., 2012; Safieddine et
20 al., 2013). Due to the rapidly changing emissions in China, the respective contribution made
21 by anthropogenic and natural perturbations to tropospheric ozone in China and its variability
22 constitutes a crucial issue to be documented and better understood. Seasonal variations in
23 ozone levels in East Asia and especially the role of the summer Asian monsoon leading to a
24 summer minimum have been extensively studied from model simulations, in situ and satellite
25 observations (e.g. Mauzerall et al., 2000; Tanimoto et al., 2005; Yamaji et al., 2006; Li et al.,
26 2007; Ding et al., 2008; Dufour et al., 2010). However, at the synoptic scale, the direct impact
27 of weather systems on tropospheric ozone distribution above China and its daily variations
28 has been less extensively considered or, if so, mainly in the scope of the long-range transport
29 of pollutants and export to the Pacific Ocean. A recent study investigates the dynamic and
30 chemical features induced in the upper troposphere by cut-off lows over northeast China
31 using limb and nadir satellite sounders (Liu et al., 2013).

1 The progress made in satellite observations of tropospheric ozone during the last decade (e.g.
2 Worden et al., 2007; Eremenko et al., 2008; Liu et al., 2010, Nakatani et al., 2012) offers a
3 new opportunity to evaluate ozone distribution and its daily variation including the role of
4 transport at the synoptic scale (e.g. Doche et al., 2014). The satellite provides an
5 unprecedented spatial coverage that allows new insight into how synoptic processes impact
6 ozone distributions. The first satellite measurements of tropospheric ozone were obtained
7 using ultraviolet-visible (UV) sounders (e.g. Fishmann et al., 2003; Liu et al., 2007). Later on,
8 the development of thermal infrared nadir sounders allowed accurate measurements of partial
9 tropospheric ozone columns to be obtained (Coheur et al., 2005; Worden et al., 2007; Dufour
10 et al., 2012; Safieddine et al., 2013). Using GOME and OMI UV sounders, Nakatani et al.
11 (2012) show a persistent belt of enhanced tropospheric columns of ozone at mid-latitudes
12 over East Asia throughout the year, partly attributed to stratospheric intrusion near the
13 subtropical jet. The tropospheric contribution to the enhanced ozone column has been
14 assessed using model simulations. Nakatani et al. (2012) underlined the difficulty in
15 differentiating the stratospheric and tropospheric origins of ozone in the tropospheric columns
16 observed by satellite. This difficulty has already been stated by de Laat et al. (2005).
17 However, it has been demonstrated that thermal infrared sounders like IASI on board MetOp
18 (Clerbaux et al., 2009) allow the retrieval of semi-independent partial columns of ozone
19 within the troposphere (Eremenko et al., 2008; Dufour et al., 2010; Dufour et al., 2012;
20 Safieddine et al., 2013; Barret et al., 2011). Dufour et al. (2010) show the ability of IASI to
21 provide independent information on the seasonal variation in lower- and upper-tropospheric
22 ozone over East Asia. Over shorter-term periods of the order of several days, the retrieved
23 ozone profile with IASI allows the identification of the origin of the observed tropospheric
24 ozone in specific cases. Very recently, Hayashida et al. (2015) show ozone enhancement in
25 the lower troposphere over East Asia using the OMI space-borne ultraviolet spectrometer.
26 They attribute the enhancement mainly to emissions of ozone precursors from open crop
27 residue burning after the winter wheat harvest.

28 In this paper, we use the IASI observation of lower-tropospheric ozone to investigate the
29 influence of synoptic scale weather systems on the distribution of ozone over East Asia. In a
30 previous study, Dufour et al. (2010) show that IASI lower-tropospheric ozone columns reach
31 a maximum in late spring and early summer (May, June) in Beijing, Shanghai and Hong
32 Kong. We then decided to focus our study on late spring (May), period during which high
33 ozone concentrations and frequent frontal activities occur over East Asia. We focus on May

Gaëlle Dufour 15/9/y 14:05

Supprimé:

Gaëlle Dufour 15/9/y 13:58

Supprimé:

Gaëlle Dufour 15/9/y 13:58

Supprimé:

1 2008, as this was the first period available with the new version of the IASI ozone product
2 used for this study. Two case studies associated with travelling low-pressure systems and
3 presenting enhanced ozone in the lower troposphere are analyzed. The first case is used to
4 elaborate the analysis method based on IASI observations of ozone (O₃) and carbon monoxide
5 (CO). We demonstrate that semi-independent ozone columns between the surface and 12 km
6 from IASI associated with simultaneous CO measurements provide a powerful observational
7 dataset to identify, at least partly, the stratospheric and anthropogenic origin of lower free
8 tropospheric ozone. The contributions made by descending air from the UTLS in the vicinity
9 of the weather systems and by the photochemical production of ozone to the enhanced lower-
10 tropospheric ozone columns are then investigated for the two case studies.

11 The paper is structured as follow. In Section 2, the different satellite and meteorological
12 datasets are described. As a new version of the IASI ozone product is used for this study, we
13 provide a summary of the validation of the product with a specific focus on East Asia in
14 Section 3. The analysis method based on ozone and CO columns is detailed in Section 4.
15 Section 5 presents the consequences of a cut-off low travelling over a highly polluted region
16 (North China Plain) in terms of ozone vertical distribution and pollutant transport. A general
17 discussion is given in Section 6 as well as a conclusion in Section 7.

18

19 **2 Datasets description**

20 **2.1 The IASI instrument**

21 The IASI (Infrared Atmospheric Sounding Interferometer) (Clerbaux et al., 2009) instrument,
22 on board the MetOp-A platform since October 2006, is a nadir-viewing Fourier transform
23 spectrometer. It operates in the thermal infrared between 645 and 2760 cm⁻¹ with an apodized
24 resolution of 0.5 cm⁻¹. The field of view of the instrument is composed of a 2 × 2 matrix of
25 pixels with a diameter at nadir of 12 km each. IASI scans the atmosphere with a swath width
26 of 2200 km and crosses the equator at two fixed local solar times 9:30 am (descending mode)
27 and 9:30 pm (ascending mode), allowing the monitoring of atmospheric composition twice a
28 day at any location. The large spectral coverage, high radiometric sensitivity and accuracy,
29 and rather high spectral resolution of the instrument allow this instrument to measure the
30 global distribution of several important atmospheric species (eg. Boynard et al., 2009; George
31 et al., 2009; Clarisse et al., 2011).

Gaëlle Dufour 15/9/y 13:58

Supprimé:

2.2 Lower-tropospheric ozone from IASI

The IASI ozone profiles and partial columns considered in this paper have been retrieved using the method described in Eremenko et al. (2008). The retrieval is performed using the radiative transfer model KOPRA (Karlsruhe Optimised and Precise Radiative transfer Algorithm) and its inversion module KOPRAFIT (Stiller et al., 2000; Höpfner et al., 2001), both adapted to the nadir-viewing geometry. A constrained least squares fit method with an analytical altitude-dependent regularization is used (Kulawik et al., 2006). The applied regularization method is detailed in Eremenko et al. (2008). To summarize, the regularization matrix is a combination of first order Tikhonov constraints (Tikhonov, 1963) with altitude-dependent coefficients. The coefficients are optimized both to maximize the degrees of freedom (DOF) of the retrieval and to minimize the total error on the retrieved profile. Compared to previous studies using this algorithm (Eremenko et al., 2008; Dufour et al., 2010, 2012), several changes have been made. The emissivity of the surface is now taken into account based on a global monthly IASI-derived climatology (Zhou et al., 2011) allowing a better retrieval above arid regions. Different a priori and constraints are used depending on the tropopause height. This new scheme was introduced to reduce possible compensation effects during the retrieval procedure. An automatic detection of the tropopause height (calculated from the temperature profile retrieved from IASI using the definition based on the lapse rate criterion (WMO, 1957)) has been introduced to discriminate between polar, midlatitudes, and tropical situations. If the tropopause is lower than 10 km, the polar constraint and a priori profile are used. If the tropopause is between 10 and 14 km, the midlatitude constraint and a priori profile are used. If the tropopause is higher than 14 km, the tropical constraint and a priori are used. The midlatitude and tropical regularization matrices are those already used in Eremenko et al. (2008) and Dufour et al. (2010, 2012) respectively. The polar constraint has been specifically developed following the same method as in Eremenko et al. (2008). The a priori profiles are compiled from the ozonesonde climatology of McPeters et al. (2007). The midlatitude a priori profile is set to the climatological profile of the 30-60°N latitude band for summer. The tropical a priori profile is set to the climatological profile of the 10-30°N latitude band over the year. The polar profile is set to the climatological profile of the 60-90°N latitude band for summer. As the version of the ozone product used in this study differs significantly from the version extensively validated in Dufour et al. (2012), a new validation against ozonesondes has been conducted and the results are presented in Section 3. The modifications of the algorithm do not influence the vertical

1 sensitivity of IASI. As shown in Dufour et al. (2010, 2012), two semi-independent partial
2 columns of ozone between the surface and 12 km can be considered: the lower-tropospheric
3 column integrating the ozone profile from the surface to 6 km altitude – above sea level (asl)
4 – and the upper-tropospheric column integrating the ozone profile from 6 to 12 km altitude.
5 Note that the latter column can include stratospheric air masses depending on the tropopause
6 height. The averaging kernels give information on the vertical sensitivity and resolution of the
7 retrieval. The lower-tropospheric column shows a maximum sensitivity typically between 3
8 and 4 km with a limited sensitivity to the surface (Dufour et al., 2012). This implies that the
9 ozone concentration profile in the lower troposphere is preferentially incremented at these
10 altitudes during the retrieval process, independently if the true ozone profile is perturbed at
11 other altitudes, especially at the surface. Moreover, it is worth noting that the partial columns
12 are only semi-independent which means that they may include partial information from
13 altitudes outside their altitude range. For example, the lower-tropospheric column includes
14 information from altitudes higher than its upper limit (6 km). In order to estimate the fraction
15 of contamination of the lower-tropospheric column by higher altitudes, we calculated the ratio
16 between the integral of the averaging kernel of the lower-tropospheric column from 6 km to
17 60 km and the integral from the surface to 60 km. Higher atmospheric layers contribute to
18 about 20 to 30 % of the lower-tropospheric column in the midlatitude air masses (not shown).
19 Note that only the morning overpasses of IASI are considered for this study in order to remain
20 in thermal conditions with a better sensitivity to the lower troposphere.

Gaëlle Dufour 15/9/y 13:59

Supprimé:

Gaëlle Dufour 15/9/y 14:05

Supprimé:

Gaëlle Dufour 15/9/y 13:59

Supprimé:

Gaëlle Dufour 15/9/y 13:59

Supprimé:

Gaëlle Dufour 15/9/y 14:00

Supprimé:

Gaëlle Dufour 15/9/y 14:00

Supprimé:

Gaëlle Dufour 15/9/y 14:00

Supprimé:

21 **2.3 Carbon monoxide from IASI**

22 The CO data used here are retrieved from the IASI spectra within the 2143-2181.25 cm^{-1}
23 spectral range using the FORLI-CO retrieval code from the Université Libre de Bruxelles
24 (ULB). FORLI-CO retrievals give CO concentration profiles using the optimal estimation
25 method (Rodgers, 2000) and a single a priori profile. More details are given in Hurtmans et al.
26 (2012). The IASI FORLI-CO product used in this study is the total column, publicly available
27 from the Ether website (<http://www.pole-ether.fr>). Note that only half of the pixels are
28 available for the year 2008. This explains the difference in measurement density between O₃
29 and CO observations in the different figures. Carbon monoxide is often used as an indicator of
30 biomass burning and anthropogenic pollution (e.g. Edwards et al., 2004; McMillan et al.,
31 2010). In this study, we use the IASI CO columns as an anthropogenic pollution tracer.

1 **2.4 Meteorological dataset**

2 Meteorological data from the ECMWF ERA-Interim reanalysis are used in our analyses. The
3 reanalysis is based on a 4D-Var assimilation system with a 12-hour analysis window. The
4 spatial resolution of the data set is approximately 80 km on 60 vertical levels from the surface
5 up to 0.1 hPa (Dee et al., 2011). In our analyses, the meteorological parameters are taken at
6 0:00 UTC, corresponding roughly to the morning overpass time of IASI. The main variables
7 considered in this study are the geopotential height, the potential vorticity (PV), and the
8 horizontal wind field (u and v components), as well as the equivalent potential temperature,
9 the vertical velocity and the convective available potential energy. The geopotential height
10 associated with horizontal wind at 850 hPa give a proxy for describing the weather situation
11 and horizontal transport in the lower troposphere, whereas the same parameters at 300 hPa
12 describe the situation in the UTLS. We also calculate the equivalent potential temperature at
13 850 hPa and 300 hPa from temperature, relative humidity and specific humidity fields
14 (Bolton, 1980) as an indicator of air masses origin (Holton, 2004). Potential vorticity (PV) is
15 often used as a tracer of tropopause height and of air masses origin (e.g. Bethan et al., 1996).
16 PV values between 1 and 1.6 PVU are representative of the upper troposphere whereas PV
17 values larger than 1.6 PVU are indicators of air mass origin above the dynamical tropopause.
18 In this study, we consider mainly PV averaged at between 300 and 500 hPa with a 50 hPa
19 interval as we are above all interested in the impact of stratospheric air masses on the free
20 troposphere. In order to investigate the ascending motion of air masses, especially from the
21 boundary layer towards the free troposphere within weather systems, we examine the vertical
22 velocity at different pressure levels as well as the convective available potential energy
23 (CAPE), which informs on the capability of the low-pressure system to vertically transport air
24 masses by convection.

25

26 **3 Validation of IASI lower-tropospheric ozone**

27 Significant changes in the ozone retrieval procedure compared to the validation exercise
28 reported in Dufour et al. (2012) have been made as described in Section 2.2. A new validation
29 exercise was done to evaluate the new version of the ozone product. We use a database of
30 ozonesonde measurements from 2007 to 2012 including 27 stations in the midlatitudinal band
31 (30-60°) in both hemispheres and 16 stations in the tropical band (30°S-30°N). Most of the
32 ozonesonde measurements are from the WOUDC (<http://woudc.org/>) and SHADOZ

Gaëlle Dufour 15/9/y 14:00

Supprimé:

1 (<http://croc.gsfc.nasa.gov/shadoz/>) databases, except for Aquila and Beijing. A list of stations
2 and related information is provided in Table 1. The coincidence criteria used for the
3 validation are 1° around the station, a time difference smaller than 6 hours and a minimum of
4 10 clear-sky pixels matching these criteria. The results of the comparison between IASI ozone
5 retrievals and ozonesonde measurements are summarized in Table 2. We focus on the lower
6 troposphere and then no correction factor has been applied on ozonesonde measurements. The
7 results for other partial columns are not significantly different compared to the previous
8 version of the product, extensively discussed by Dufour et al. (2012). The bias for the lower-
9 tropospheric column (surface to 6 km asl) is small -0.6 DU (-2.8%) and comparable to the
10 bias estimated at the midlatitudes with the previous version of the product (Dufour et al.,
11 2012). The estimated error is about 2.8 DU (14%) with a correlation coefficient of 0.70. Table
12 2 also summarizes the results for East Asian ozonesonde stations only (Beijing, Hong Kong,
13 Sapporo and Tateno). A significant bias of 2.2 DU (9.5%) with IASI underestimating ozone
14 partial columns is determined. The bias is similar for Beijing, Hong Kong, and Tateno (-2.6
15 DU) and different for Sapporo (+0.8 DU). Most of the ozonesonde measurements are
16 performed in the early afternoon. The ozone build-up is then maximal in polluted urban or
17 suburban sites like Beijing, Hong Kong, and Tateno. IASI observations are performed in the
18 morning, about 5 hours earlier on average. The time difference between IASI and ozonesonde
19 observations in polluted suburban sites may partly explain the larger bias in this case. Indeed,
20 the bias for the Sapporo region, where the diurnal cycle of ozone is limited, is reduced.
21 However, the small number of coincidences does not allow any firm conclusion to be reached
22 on the origin of the observed bias over East Asia.

23

24 **4 Case study of 4-6 May 2008: on the use of IASI O₃ and CO to diagnose the** 25 **processes influencing the ozone distribution affected by weather systems**

26 An episode of high ozone is observed in the lower troposphere with IASI in North East Asia
27 from 4 to 6 May 2008. This episode is associated with a low-pressure system travelling from
28 Mongolia through North China to the extreme north of Japan. In this section, we investigate
29 how to use the ozone partial columns and profiles and the CO total columns from IASI to
30 diagnose which processes contribute to the ozone enhancement.

Gaëlle Dufour 15/9/y 14:00

Supprimé:

1 4.1 Low-pressure system and associated IASI ozone distribution

2 Figure 1 describes the meteorological situation of this episode of high ozone. A large cold
3 front extending from Mongolia to South China on 4 May 2008, from North China to the
4 Southern Japanese Islands on 5 May 2008, and moving eastward from Japan on 6 May 2008
5 characterizes the low-pressure system (Figs. 1a-c). The regions behind the frontal area and
6 north to the polar jet, situated between 35°N and 40°N on these dates (Figs. 1d-f), are strongly
7 influenced by polar air masses with tropopause heights below 9 km (Figs. 1g-i). The 300-500
8 hPa mean PV values are larger than 1.6 PVU for the same regions, indicating that the upper
9 troposphere is under the influence of lower stratospheric air masses (Figs. 2j-l). The spatial
10 correlation of low tropopauses and large PV values indicates that reversible subsiding ozone
11 transfer affects the upper troposphere in this case. We then expect an ozone enhancement in
12 the upper troposphere for these regions and we will see in the following how IASI describes
13 this ozone enhancement induced by ozone subsidence. The analysis of the upper-tropospheric
14 columns shows that IASI observes columns larger than 40 DU in the regions affected by low
15 tropopauses and large PV (Figs 2g-i). A step gradient between 30 and 40 DU is observed in
16 the upper-tropospheric ozone distribution reflecting the step gradient in the PV distribution.
17 The very good spatial correlation of the high UT ozone structures with those of high PV leads
18 us to consider that the upper-tropospheric columns of ozone retrieved from IASI can be used
19 as a proxy to determine the regions affected by subsiding ozone from the lower stratosphere.
20 The threshold of 40 DU seems to be relevant for this identification.

21 The question now is to determine to what extent IASI is able to inform about the low-pressure
22 system's influence on the lower-tropospheric ozone distribution. The physical processes,
23 which may affect the lower-tropospheric ozone distribution, are (i) the reversible ozone
24 subsidence associated with low tropopause heights, which induces an enhancement of ozone
25 in the upper and free troposphere, and then partly in the lower troposphere; (ii) irreversible
26 stratosphere-troposphere exchanges, which also lead to ozone enhancement. The first process
27 is expected to affect ozone distribution at a synoptic scale whereas the second process is more
28 localized. Figures 2a-c show that lower-tropospheric ozone columns larger than 28 DU are
29 observed with IASI in the vicinity of the low with similar spatial patterns to the UT columns
30 and the PV distribution. The observed enhancement in the lower-tropospheric column
31 (surface-6km) arises from 1) the actual (reversible) transfer of ozone to the free troposphere,
32 2) the definition of the LT columns by itself, 3) the limited vertical resolution of the retrieval

Gaëlle Dufour 15/9/y 14:06

Supprimé:

Gaëlle Dufour 15/9/y 14:06

Supprimé:

Gaëlle Dufour 15/9/y 14:06

Supprimé:

Gaëlle Dufour 15/9/y 11:53

Mis en forme: Normal, Sans numérotation ni puces

Gaëlle Dufour 15/9/y 14:00

Supprimé:

Gaëlle Dufour 15/9/y 14:00

Supprimé:

Gaëlle Dufour 15/9/y 14:01

Supprimé:

Gaëlle Dufour 15/9/y 14:01

Supprimé:

Gaëlle Dufour 15/9/y 11:51

Supprimé: -

Gaëlle Dufour 15/9/y 11:51

Supprimé: ; -

1 and the associated smoothing of the vertical profile. Indeed, the LT columns are defined as
2 the columns from the surface up to 6 km. Consequently, when the tropopause is low (below 9
3 km), the LT column arithmetically includes layers with upper-tropospheric characteristics.
4 Moreover, due to the limited vertical resolution of the retrieval and the associated smoothing
5 of the vertical profile, the lower-tropospheric column is partly contaminated by ozone outside
6 the column altitude boundaries, as discussed in Section 2.2. This may contribute to an
7 overestimation of the lower-tropospheric column. However, it is difficult to estimate this
8 overestimation in our case because no ozonesonde observations were available along the path
9 of the low.

10 We show with this case study that having the IASI UT and LT ozone columns allows us to
11 determine those regions affected by the subsiding transfer of ozone occurring behind the
12 frontal area and if the lower troposphere is affected. Now, we will examine if and how IASI
13 can be used to characterize irreversible stratosphere-troposphere exchanges (STE). The
14 analysis of the PV distribution at different pressure levels allows the identification of the
15 region in the vicinity of the low where STE occurs. In the case study from 4 to 6 May 2008,
16 we identify two regions with high PV values down to 600 or 500 hPa on the path of the low
17 (not shown): one on the east coast of Korea on 5 May (~39°N, 128°E) and one offshore to the
18 northeast of Tokyo (~39°N, 142.5°E). The STE is situated in the southeast flank of the low-
19 pressure system, behind and in the southern part of the cold front in the two cases. Figure 3
20 displays the longitudinal and latitudinal vertical section of ozone at 128°E and 39°N for 5
21 May (top) and at 142.5°E and 39°N for 6 May (bottom). On 5 May, strong stratospheric
22 intrusion of ozone is observed between 38°N and 39°N, and between 125°E and 130°E. The
23 vertical section at 128°E shows that the free and lower troposphere are still connected to the
24 polar UTLS reservoir that day. On 6 May, a stratospheric intrusion is observed between 36°N
25 and 38°N, and between 140°E and 143°E. The vertical section along 142°E shows that the
26 enhanced ozone in the lower troposphere (below 7 km) is partly disconnected from the polar
27 UTLS reservoir. Backtrajectories performed with the HYSPLIT trajectory model (Draxler and
28 Rolph; Rolph) show that the 3km-altitude air masses located in this area originate from
29 altitudes between 5 and 7 km the day before from North China and Inner Mongolia (Fig. S1).
30 The tropopause height was around 7-8 km on 5 May 2008 for these regions (Fig. 1h). This
31 means that the air masses reaching northeast of Tokyo at 3 km on 6 May have a UTLS origin
32 and transport ozone-rich air into the lower troposphere. Thus, we show that the downward
33 transport from the UTLS affects ozone concentrations in the lower troposphere for specific

Gaëlle Dufour 15/9/y 11:51

Supprimé: . The upper boundary of the column is fixed at 6 km. W

Gaëlle Dufour 15/9/y 14:06

Supprimé:

Gaëlle Dufour 15/9/y 11:54

Supprimé: . As discussed in Section 2.2

Gaëlle Dufour 15/9/y 14:01

Supprimé:

Gaëlle Dufour 15/9/y 11:54

Supprimé: then

Gaëlle Dufour 15/9/y 14:01

Supprimé:

1 regions on the southeastern flank of the weather system, whereas the perturbation of the
2 tropopause associated with this system influences upper and lower-tropospheric ozone over
3 larger areas in the vicinity of the low.

Gaëlle Dufour 15/9/y 14:01

Supprimé:

4 **4.2 Influence of the high-pressure system on tropospheric ozone distribution** 5 **over the NCP**

6 On 5 May 2008, an anticyclone is forming over Central East China and the North China Plain.
7 The northwesterly winds reaching the NCP change progressively to southwesterly winds from
8 4 to 6 May with low winds and then a stagnant situation on 5 May (Figs. 1a-c). This,
9 associated with low cloud coverage and then increasing radiation, is a situation favorable to
10 the accumulation of primary pollutants over the NCP and to the photochemical production of
11 ozone due to both local emissions and regional transport of pollutants. The question here is
12 how IASI is able to describe this situation. The CO columns observed with IASI show
13 enhanced values over the NCP on 5 and 6 May (Figs. 2e and 2f). Considering CO as a
14 pollution tracer, enhanced IASI CO columns can be used to evaluate the build-up of
15 pollutants. Concomitantly, lower-tropospheric ozone columns as large as 30 DU are observed
16 (Figs. 2b and 2c). A significant spatial correlation ($r=0.6$) is calculated between CO and
17 lower-tropospheric ozone columns for a square region including the NCP ($35-41^{\circ}\text{N}$, $114-$
18 122°E) on 5 May. In addition, the upper-tropospheric ozone column does not show enhanced
19 values over the NCP for these 2 days (Figs. 2h and 2i). The analysis of the vertical section of
20 ozone distribution on 5 May shows that the large ozone concentrations in the Beijing region
21 (Fig. 3, $\sim 39^{\circ}\text{N}$ and $\sim 116^{\circ}\text{E}$) and across the NCP are retrieved below 6 km and are
22 disconnected from the UTLS region. The maximal values of ozone are retrieved between 2
23 and 3 km over Beijing (Fig. 3) in agreement, considering the vertical sensitivity and
24 resolution of IASI, with in situ measurements, which frequently report high ozone
25 concentrations at an altitude of 1.5-2km above Beijing during April-May (Huang et al., 2014).
26 This associated with the correlation with CO suggests that the enhanced ozone observed with
27 IASI is mainly due to the photochemical transformation of primary pollutants emitted over
28 the NCP. To evaluate the degree of photochemical production of ozone, we calculate the
29 equivalent or mean mixing ratio corresponding to the CO and LT O₃ columns. This allows us
30 to estimate a relative enhancement ratio of O₃ to CO of 0.14 and 0.08 on 5 and 6 May
31 respectively. These values are in agreement with the typical values ranging between 0 and 0.3

Gaëlle Dufour 15/9/y 14:01

Supprimé:

Gaëlle Dufour 15/9/y 14:02

Supprimé:

Gaëlle Dufour 15/9/y 14:06

Supprimé:

1 reported over East Asia by Tanimoto et al. (2008). The estimated enhancement ratio remains
2 quite low suggesting an early stage of ozone production.

3

4 **5 Case study of 11-16 May 2008: combined contributions of anthropogenic** 5 **and stratospheric sources over the NCP and pollution transport**

6 A second episode of high ozone is observed in the lower troposphere over the North China
7 Plain (NCP) from 11 to 16 May 2008. This episode is associated with a cut-off low-pressure
8 system forming on 11 May over Inner Mongolia and moving east on subsequent days. From
9 14 May, the meteorological regime changes over the NCP with warmer air masses settling
10 within an anticyclonic situation. In this section, we examine the influence of the
11 meteorological situation on the distribution of lower and upper-tropospheric ozone with a
12 particular focus on the NCP. Figure 4 describes the meteorological situation for the entire
13 period. Figures 5 and 6 display the lower and upper-tropospheric ozone columns and the total
14 CO columns observed with IASI.

15 **5.1 11-13 May: NCP under the direct influence of the cut-off low**

16 On 11 May 2008, a cut-off low is forming over Inner Mongolia (Fig. 4a). The cut-off low is
17 not yet completely dissociated from the polar reservoir. A band of upper-tropospheric
18 columns larger than 40 DU is observed by IASI between 35°N and 45°N (Fig. 5g). As seen in
19 Section 4, it indicates that the region is under the influence of subsiding ozone. The lower-
20 tropospheric ozone columns do not show a clear enhancement for the same latitude band. On
21 that day, subsiding ozone affects only moderately the lower-tropospheric ozone.

22 On 12 May 2008, the cut-off low is well dissociated from the western current and its center
23 reaches the Bohai Sea (Fig. 4b). Upper-tropospheric ozone columns larger than 45 DU are
24 retrieved all around the cut-off low. Lower-tropospheric ozone columns larger than 32 DU are
25 observed especially in the southwestern part of the low, just above the NCP (Fig. 5b). The
26 analysis of the vertical section of ozone at 117°E (Fig. 7a) shows that the subsiding transfer of
27 ozone due to the tropopause perturbation strongly affects lower-tropospheric ozone north of
28 33°N. At 32°N, the ozone enhancement observed in the lower troposphere is not connected to
29 the UTLS reservoir, suggesting a possible photochemical origin for this enhancement. IASI
30 CO columns are also enhanced in the NCP region and partly correlated with the enhanced

Gaëlle Dufour 15/9/y 14:06

Supprimé:

Gaëlle Dufour 15/9/y 14:06

Supprimé:

Gaëlle Dufour 15/9/y 14:07

Supprimé:

Gaëlle Dufour 15/9/y 14:02

Supprimé:

Gaëlle Dufour 15/9/y 14:02

Supprimé:

Gaëlle Dufour 15/9/y 14:07

Supprimé:

Gaëlle Dufour 15/9/y 14:02

Supprimé:

Gaëlle Dufour 15/9/y 14:02

Supprimé:

1 ozone columns (Fig. 5e). This indicates that pollution likely plays a concomitant role in the
2 ozone enhancement in that case.

3 On 13 May 2008, the centre of the cut-off low moves slightly to the East and reaches the
4 Yellow Sea (Fig. 4c). As for the previous day, large upper and lower-tropospheric ozone
5 columns are observed with IASI in the vicinity of the low (Figs. 5c and 5i). The two columns
6 are slightly smaller than the day before over the NCP. The analysis of the vertical section of
7 ozone at 115°E (Fig. 7b) shows that the subsiding transfer of ozone due to the tropopause
8 perturbation is less effective than the previous day. Even if the lower-tropospheric ozone
9 remains partly connected to the UTLS reservoir north of 33°N, secondary maxima are
10 observed at ~4 km of altitude, suggesting that an additional source of ozone may contribute to
11 the LT ozone enhancement. South of 33°N the ozone enhancement is clearly located in the
12 lower troposphere. The good spatial correlation of LT ozone enhancement and the strong CO
13 enhancement observed all over the NCP (Fig. 5f) confirms that pollution plays a concomitant
14 role in explaining the ozone distribution in the lower troposphere over the NCP for this day.

15 **5.2 14 May: transition from a cyclonic to an anticyclonic situation**

16 On 14 May 2008, the cut-off low shifts to the Sea of Japan (Fig. 4d). A large area including
17 North China, Korea, and reaching Japan shows upper-tropospheric columns larger than 40
18 DU (Fig. 6g), which indicates the region is under the influence of subsiding ozone. Within
19 this area, the largest LT ozone columns are observed in an area less extended and situated on
20 the southeastern flank of the low, mainly over the Sea of Japan (Fig. 6a). The lower
21 troposphere is then certainly under the influence of the UTLS.

22 Over China, an anticyclonic situation starts to develop south of the NCP inducing a change in
23 the wind regime and warmer conditions from 14 May (Fig. 4d). Enhanced CO columns and
24 lower-tropospheric ozone columns are retrieved with IASI over the NCP (Figs. 6a and 6d)
25 with moderate UT ozone columns. The analysis of the vertical section of ozone
26 concentrations at 35°N shows that very large ozone concentrations are retrieved for the entire
27 free and upper troposphere in the eastern part of the section (Fig. 7c). This corresponds to the
28 region over the Sea of Japan under the direct influence of the cut-off low and then greatly
29 influenced by the UTLS. The situation is different over the NCP: ozone concentrations in the
30 upper troposphere are moderate and a distinct maximum in the lower troposphere is clearly
31 visible. This, associated with CO enhancement over the NCP in good spatial correlation with

Gaëlle Dufour 15/9/y 14:02

Supprimé:

Gaëlle Dufour 15/9/y 14:02

Supprimé:

Gaëlle Dufour 15/9/y 14:07

Supprimé:

Gaëlle Dufour 15/9/y 14:03

Supprimé:

1 LT ozone, indicates that the ozone enhancement observed with IASI over the NCP is of
2 anthropogenic origin and related to the photochemical production of ozone. On that day, the
3 estimated enhancement ratio of O₃ to CO is 0.11 in agreement with the enhancement ratio
4 calculated for the previous case study.

5 **5.3 15-16 May: NCP under anticyclonic influence**

6 On 15 and 16 May 2008, strong enhancements of CO and lower-tropospheric ozone are
7 observed with IASI over the entire NCP (Figs. 6b-c and 6e-f). Both CO and O₃ increase
8 compared to the previous day. The anticyclone is firmly settled over China, leading to a
9 stagnant situation with low winds all over the NCP (Fig. 4e). This situation is favorable to the
10 accumulation of pollutant and then to the photochemical production of ozone. Figure 7d
11 shows the vertical section of ozone concentrations retrieved with IASI at 37°N. The ozone
12 enhancement is located below 4 km, especially between 115°E and 116°E, in agreement with
13 the findings of Section 4.2. This, with CO enhancement, indicates that the ozone enhancement
14 is due to photochemical production from pollutants emitted in the NCP. In this case of
15 stronger CO enhancement, the enhancement ratio of O₃ to CO (0.09 on 15 May and 0.06 on
16 16 May) decreases compared to the previous days.

17 **5.4 Evidence of transboundary transport within the cut-off low**

18 On 13 and 14 May, large CO and O₃ columns are retrieved from IASI over the Yellow Sea
19 and over the Sea of Japan on the southern flank of the cut-off low-pressure system (Figs. 5c
20 and 6a). Fairly strong westerly winds are present at 850 hPa in the same region, suggesting a
21 possible advection of air masses from the NCP towards Japan associated with the weather
22 system (Figs. 4c and 4d). In order to assess whether the weather system may have contributed
23 to transporting the pollutants (O₃ and CO), we perform backtrajectories on 13 May for an area
24 south to Korea (Fig. S2). The 3-km air masses originate from the boundary layer over NCP
25 on 11 May. They have been uplifted and transported at an altitude of between 3 and 4 km on
26 subsequent days (Fig. S2). In order to investigate if the pollutant uplifting on 11 May occurs
27 over a region more extended than those shown on Fig. S2, we examined two meteorological
28 variables that indicate possible ascending motion of air masses: the convective available
29 potential energy (CAPE) and the vertical velocity. Figure 8 shows that CAPE is significant on
30 the inside eastern flank of the cut-off low and that negative vertical velocities, i.e., ascending
31 winds, are present from the surface up to 300 hPa (Fig. 8 shows only the vertical velocity at

Gaëlle Dufour 15/9/y 14:03

Supprimé:

1 700 hPa as an example). In addition, backtrajectories performed on 11 May indicate that most
2 of the air masses between 38-40°N and 116-117°E at 3 km originate from the atmospheric
3 layers below 1 km and circulate over the NCP during the previous 24 hours (Fig. S3). This
4 evidences that pollutants (CO and O₃) have been uplifted from the boundary layer into the
5 free troposphere over NCP and then exported towards Japan by the cut-off low. This transport
6 pathway is relatively well known. Very recently, Ding et al. (2015) studied in detail the
7 uplifting and transport of CO in East Asia. They show that the vertical transport of
8 anthropogenic CO originating from the NCP is mainly carried out by frontal lifting associated
9 or not with WCB. They also pointed out the additional topography's role in the CO lifting
10 over the NCP.

11 To complete the study, we calculate the enhancement ratio of O₃ to CO over NCP on 12 May,
12 over the Yellow Sea and Korea (32-36°N, 122-130°E) on 13 May, and over the Sea of Japan
13 (30-38°N, 128-140°E) on 14 May. The ratios are respectively 0.16, 0.21 and 0.28. The
14 increase of the ratio indicates possible photochemical processing during the transport. Part of
15 the large lower-tropospheric ozone is then due to the transport of ozone produced over the
16 NCP but also to ozone produced during the transport.

17

18 **6 Role of weather systems and photochemical production at the monthly** 19 **timescale**

20 The succession of low- and high-pressure systems plays a key role in explaining the day-to-
21 day variations of lower-tropospheric ozone over North East Asia. In May 2008, 5 events
22 covering 2-3 days each and leading to significant ozone enhancement in the lower
23 troposphere have been identified. In order to evaluate the regions of influence of the frontal
24 and cyclonic activity on the ozone distribution, we calculated monthly means of lower and
25 upper-tropospheric ozone columns (Fig. 9). The monthly means are given with a 0.25°x0.25°
26 horizontal resolution. The upper-tropospheric ozone columns are the most affected by the
27 ozone subsiding transfer induced by the tropopause perturbations associated with frontal
28 activity. Looking at UT ozone columns larger than 40 DU provides a view of the region of
29 influence of the frontal and cyclonic activity in terms of ozone enhancement. This region is
30 located north of 40°N and extends from Inner Mongolia to North China and the North of
31 Japan. South of 40°N, the influence of the frontal and cyclonic activity on lower-tropospheric
32 ozone decreases.

Gaëlle Dufour 15/9/y 14:03

Supprimé:

Gaëlle Dufour 15/9/y 11:58

Supprimé: Discussion

Gaëlle Dufour 15/9/y 14:03

Supprimé:

Gaëlle Dufour 15/9/y 14:07

Supprimé:

Gaëlle Dufour 15/9/y 14:07

Supprimé:

Gaëlle Dufour 15/9/y 14:03

Supprimé:

1 In order to investigate the role of pollution in enhanced lower-tropospheric ozone columns
2 observed with IASI, we compare monthly distribution of lower-tropospheric ozone columns
3 with the distribution of total CO columns and tropospheric NO₂ columns, often used as
4 anthropogenic sources tracers (Fig.9). The NO₂ tropospheric columns are those observed by
5 the GOME-2 instrument operating on the same satellite platform than the IASI instrument
6 (Boersma et al., 2004) (<http://www.temis.nl/airpollution/no2.html>). All the regions of
7 continental East Asia (NCP, Sichuan Basin, North China...) showing large NO₂ tropospheric
8 columns and then indicating large anthropogenic sources present large total CO columns and
9 also large lower-tropospheric ozone columns (Fig. 9). A correlation of 0.62 over the entire
10 domain between IASI lower-tropospheric ozone and IASI total CO suggests that
11 anthropogenic sources significantly contribute to the ozone observed in the lower troposphere
12 with IASI. The North China Plain, Yangtze River Delta (near Shanghai) and Hubei province
13 (Wuhan region) are the regions most impacted by pollution according to the satellite
14 observations. Large lower-tropospheric ozone columns are observed over North China
15 corresponding to the industrialised Shenyang-Harbin axis also visible in CO and NO₂
16 observations (Fig. 9). However, the ozone plume extends more to the west compared to the
17 CO and NO₂ plumes. This may be explained by the influence of the UTLS, which is larger all
18 over the northern part of the domain. Lower-tropospheric columns of ozone might also be
19 overestimated during the retrieval because the region is partly arid. Indeed, the ozone retrieval
20 can be partly impacted in regions of low emissivity. In the southern part of the domain,
21 enhanced lower-tropospheric ozone columns are observed in the Sichuan Basin and
22 Guangdong province in coincidence with enhanced CO and NO₂ columns. In this latter
23 region, closer to the equator, the distance between two successive swaths of IASI increases.
24 Then, the spatial and temporal coverage of IASI decreases and it is then less easy to follow
25 the daily variations of ozone. Moreover, the maximum of sensitivity of IASI ozone retrievals
26 in the tropics is usually higher in altitude around 5 km (Dufour et al., 2012). IASI
27 observations are then less suitable to efficiently monitor pollution in such cases.

28

29 7 Conclusion

30 Based on ozone and CO retrieval from IASI, we elaborate an analysis method to diagnose
31 which processes contribute to ozone enhancement in the lower troposphere. We demonstrate
32 that ozone profiles and semi-independent ozone columns between the surface and 12 km

Gaëlle Dufour 15/9/y 14:03

Supprimé:

Gaëlle Dufour 15/9/y 14:03

Supprimé:

Gaëlle Dufour 15/9/y 14:04

Supprimé:

Gaëlle Dufour 15/9/y 14:04

Supprimé:

Gaëlle Dufour 15/9/y 14:04

Supprimé:

Gaëlle Dufour 15/9/y 14:04

Supprimé:

Gaëlle Dufour 15/9/y 14:04

Supprimé:

Gaëlle Dufour 15/9/y 13:48

Supprimé: We apply the method to evaluate the respective role of the stratospheric and the photochemical sources of ozone on the day-to-day variation of the lower tropospheric ozone distribution over East Asia. The study allows us to stress how satellite observations can help in monitoring and identifying these different sources. We focus on late springtime because the cyclonic activity – well known to drive the stratosphere-troposphere exchanges – is important and the photochemical production of ozone in polluted areas can be significant at this time of the year.

1 associated with simultaneous CO measurements from IASI provide a powerful observational
2 dataset to identify the stratospheric and anthropogenic origin of the lower-tropospheric ozone.

3 We show that UT ozone columns larger than 40 DU are a proxy to identify the region of
4 subsiding ozone associated with the tropopause perturbation induced by low-pressure weather
5 systems. Combined with LT ozone columns larger of ~30 DU, it identifies the areas in the
6 lower troposphere affected by the UTLS reservoir of ozone. We show that the ozone
7 subsiding transfer due to the tropopause perturbations associated with the low-pressure
8 systems affect the free and lower-tropospheric ozone over large regions. We determine the
9 region of influence of such systems, located mainly above 40°N but with some particular
10 intense events (e.g. cut-off low from 11 to 13 May 2008) impacting southern regions such as
11 the NCP for few days. The vertical dimension provided by IASI allows the identification of
12 the STE areas, which are located in the southern part behind the cold front in the case of the
13 frontal system and on the southern or southeastern flanks of the low in the case of a cut-off
14 low. Note that the STE are expected to occur preferentially on the western and southern flanks
15 of the trough.

16 Based on the case of a cut-off low travelling over the NCP from 11 to 14 May 2008, we show
17 that such systems, with potential convective capacity, when they travel over highly polluted
18 regions, play a key role in the transboundary transport of pollutants. We identify from the
19 O₃/CO enhancement ratio estimated from IASI observations that significant ozone
20 photochemical production occurs during the transport from the NCP on 12 May to the Sea of
21 Japan on 14 May.

22 On the contrary, we show that large LT ozone columns when not associated with large UT
23 ozone columns but with enhanced CO total columns – used as a pollution tracer – indicate the
24 areas where the photochemical production of ozone forms part of the observed ozone
25 enhancement in the lower troposphere. Most of the enhanced lower-tropospheric ozone
26 columns are observed in regions mainly impacted by strong pollution level. Significant
27 correlations between CO (used as a pollution tracer) and ozone in the lower troposphere have
28 been found as well as enhancement ratio of O₃ to CO, consistent with those from literature.

29 Moreover, the analysis of vertical sections of ozone concentrations over NCP indicates that
30 ozone concentrations are enhanced only in the lower troposphere in such regions, indicating
31 the anthropogenic origin of the observed ozone enhancements. The maximal values of ozone
32 are observed between 2 and 4 km in cases where an anticyclonic situation is well settled over

Gaëlle Dufour 15/9/y 14:04

Supprimé:

Gaëlle Dufour 15/9/y 13:49

Supprimé: One of the advantages of IASI is to provide 3-dimensional observations of ozone distribution at synoptic scale when cloud free. The analysis of vertical section in longitude or latitude allows one to identify more precisely the areas where the lower troposphere is connected to the UTLS reservoir and the region of possible irreversible stratosphere-troposphere exchanges.

Gaëlle Dufour 15/9/y 13:51

Supprimé: Once again, the 3D observational capability of IASI (vertical sections) allows one to evaluate if the ozone enhancement observed in the LT is disconnected from the UTLS reservoir and thus to assess the anthropogenic origin of the LT ozone enhancement or the mixing of the sources. We also show that

Gaëlle Dufour 15/9/y 13:53

Supprimé: , can be derived from IASI. - ... [1]

1 the NCP (e.g. 5 and 15 May 2008). This is in agreement with in situ measurements (Huang et
2 al., 2014), considering the limited vertical resolution of IASI and its limited sensitivity to
3 surface ozone. Because of these limitations, it is not possible to determine more precisely the
4 altitude of the ozone enhancements in the troposphere. This is all the more penalizing when
5 stratospheric and photochemical events occur at the same time. The lack of vertical resolution
6 does not allow the various contributions to be differentiated. Combined with modelling
7 studies, advanced satellite products coupling UV and IR information such as the recent
8 IASI+GOME-2 product (Cuesta et al., 2013) as well as the next generation of satellite
9 instruments (Crevoisier et al., 2014, Veefkind et al., 2012) should help assessing this issue.

10

11 **Acknowledgements**

12 We acknowledge the Institut für Meteorologie und Klimaforschung (IMK), Karlsruhe,
13 Germany, for a licence to use the KOPRA radiative transfer model. This study was supported
14 by the French Space Agency - CNES (project “IASI-TOSCA”). The IASI mission is a joint
15 mission of Eumetsat and the Centre National d’Etudes Spatiales (CNES, France). The IASI
16 L1 data are distributed in near real time by Eumetsat through the Eumetcast system
17 distribution. We acknowledge the Ether CNES/CNRS-INSU database ([http://www.pole-](http://www.pole-ether.fr)
18 [ether.fr](http://www.pole-ether.fr)) for providing access to IASI Level 1 data. We acknowledge the LATMOS/ULB for
19 the provision of IASI CO total columns through the Ehter CNES/CNRS-INSU database. The
20 authors gratefully acknowledge the NOAA Air Resources Laboratory (ARL) for the provision
21 of the HYSPLIT transport and dispersion model and/or READY website
22 (<http://www.ready.noaa.gov>) used in this publication. We acknowledge the free use of
23 tropospheric NO₂ column data from the GOME-2 sensor from www.temis.nl. The
24 ozonesonde data used in this study were mainly provided by the World Ozone and Ultraviolet
25 Data Centre (WOUDC), the Southern Hemisphere Additional Ozonesondes (SHADOZ), and
26 the Global Monitoring Division (GMD) of NOAA’s Earth System Research Laboratory and
27 are publicly available (see <http://www.woudc.org>, <http://croc.gsfc.nasa.gov/shadoz>,
28 <http://www.esrl.noaa.gov/gmd>). The authors thank all those responsible for the WOUDC,
29 SHADOZ, and GMD measurements and archives for making the ozonesonde data available.

30

31 **References**

1 Ancellet, G., Beekmann, M., and Papayannis, A.: Impact of a cut-off low development on
2 downward transport of ozone in the troposphere, *J. Geophys. Res.* 99, 3451-3468, 1994.

3 Barret, B., Le Flochmoen, E., Sauvage, B., Pavelin, E., Matricardi, M., and Cammas, J. P.:
4 The detection of post-monsoon tropospheric ozone variability over south Asia using IASI
5 data, *Atmos. Chem. Phys.*, 11, 9533-9548, doi:10.5194/acp-11-9533-2011, 2011.

6 Bethan, S., Vaughan, G. and Reid, S. J.: A comparison of ozone and thermal tropopause
7 heights and the impact of tropopause definition on quantifying the ozone content of the
8 troposphere. *Q.J.R. Meteorol. Soc.*, 122: 929–944. doi: 10.1002/qj.49712253207, 1996

9 Bethan, S., Vaughan, G., Gerbig, C., Volz-Thomas, A., Richer, H., and Tiddeman, D. A. :
10 Chemical air mass differences near fronts, *J. Geophys. Res.*, 103, D11, 13413-13434, 1998.

11 Bey, I., Jacob, D. J., Logan, J. A., and Yantosca, R. M. : Asian chemical outflow to the
12 Pacific in spring : Origins, pathways, and budgets, *J. Geophys. Res.*, 106, D19, 23097-23113,
13 2001.

14 Boersma, K.F., Eskes, H.J. and Brinksma, E.J.: Error Analysis for Tropospheric NO₂
15 Retrieval from Space, *J. Geophys. Res.*, 109, D04311, doi:10.1029/2003JD003962, 2004.

16 Bolton, D. : The computation of equivalent potential temperature, *Mon. Wea. Rev.*, 108,
17 1046–1053, 1980.

18 Boynard, A., Clerbaux, C., Coheur, P.-F., Hurtmans, D., Turquety, S., George, M., Hadji-
19 Lazaro, J., Keim, C., and Meyer-Arnek, J.: Measurements of total and tropospheric ozone
20 from IASI: comparison with correlative satellite, ground-based and ozonesonde observations,
21 *Atmos. Chem. Phys.*, 9, 6255–6271, doi:10.5194/acp-9-6255-2009, 2009.

22 Carmichael, G. R., Uno, I., Phadnis, M. J., Zhang, Y., and Sunwoo, Y. : Tropospheric ozone
23 production and transport in the springtime in east Asia, *J. Geophys. Res.*, 103,10649-10671,
24 1998.

25 Chan, C. K., and Yao, X., Air pollution in mega cities in China, *Atmos. Env.*, 42, 1-42, 2008.

26 Clarisse, L., R'Honi, Y., Coheur, P.-F., Hurtmans, D., and Clerbaux, C.: Thermal infrared
27 nadir observations of 24 atmospheric gases, *Geophys. Res. Lett.*, 38, L10802,
28 doi:10.1029/2011GL047271, 2011.

29 Clerbaux, C., Boynard, A., Clarisse, L., George, M., Hadji-Lazaro, J., Herbin, H., Hurtmans,
30 D., Pommier, M., Razavi, A., Turquety, S., Wespes, C., and Coheur, P.-F.: Monitoring of

1 atmospheric composition using the thermal infrared IASI/MetOp sounder, *Atmos. Chem.*
2 *Phys.*, 9, 6041–6054, doi:10.5194/acp-9-6041-2009, 2009.

3 Crevoisier, C., C. Clerbaux, V. Guidard, T. Phulpin, R. Armante, B. Barret, C. Camy-Peyret,
4 J.-P. Chaboureau, P.-F. Coheur, L. Crépeau, G. Dufour, L. Labonnote, L. Lavanant, J. Hadji-
5 Lazaro, H. Herbin, N. Jacquinet-Husson, S. Payan, E. Péquignot, C. Pierangelo, P. Sellitto,
6 and C. Stubenrauch, Towards IASI-New Generation (IASI-NG): impact of improved spectral
7 resolution and radiometric noise on the retrieval of thermodynamic, chemistry and climate
8 variables, *Atmos. Meas. Tech.*, 7, 4367-4385, 2014

9 Coheur, P.-F., Barret, B., Turquety, S., Hurtmans, D., Hadji-Lazaro, J., and Clerbaux, C.:
10 Retrieval and characterization of ozone vertical profiles from a thermal infrared nadir
11 sounder, *J. Geophys. Res.*, 110, D24303, doi:10.1029/2005JD005845, 2005.

12 Cooper, O. R., Moody, J. L., Davenport, J. C., Oltmans, S. J., Johnson, B. J., Chen, X.,
13 Shepson, P. B., and Merrill, J. T. : Influence of springtime weather systems on vertical ozone
14 distribution over three North American sites, *J. Geophys. Res.*, 103, 22001-22013, 1998.

15 Cooper, O. R., Moody, J. L., Parrish, D. D., Trainer, M., Holloway, J. S., Hübler, G.,
16 Fehsenfeld, F. C., and Stohl, A. : Trace gas composition of midlatitude cyclones over the
17 western North Atlantic Ocean : A seasonal comparison of O₃ and CO, *J. Geophys. Res.*, 107,
18 D7, 4057, 10.1029/2001JD000902, 2002a.

19 Cooper, O. R., Moody, J. L., Parrish, D. D., Trainer, M., Ryerson, T. B., Holloway, J. S.,
20 Hübler, G., Fehsenfeld, F. C., and Evans, M. J. : Trace gas composition of midlatitude
21 cyclones over the western North Atlantic Ocean : A conceptual model, *J. Geophys. Res.*, 107,
22 D7, 4056, doi :10.1029/2001JD000901, 2002b.

23 Cooper, O. R., Forster C., Parrish, D., Trainer, M., Dunlea, E., Ryerson, T., Hübler, G.,
24 Fehsenfeld, F., Nicks, D., Holloway, J., de Gouw, J., Warneke, C., Roberts, J. M., Flocke, F.,
25 and Moody, J. : A case study of transpacific warm conveyor belt transport : Influence of
26 merging airstreams on trace gas import to North America, *J. Geophys. Res.*, 109, D23S08,
27 doi :10.1029/2003JD003624, 2004.

28 Cuesta, J., Eremenko, M., Liu, X., Dufour, G., Cai, Z., Höpfner, M., von Clarmann,
29 T., Sellitto, P., Foret, G., Gaubert, B., Beekmann, M., Orphal, J., Chance, K., Spurr, R.,
30 and Flaud, J.-M.: Satellite observation of lowermost tropospheric ozone by multispectral
31 synergism of IASI thermal infrared and GOME-2 ultraviolet measurements over Europe,

1 Atmos. Chem. Phys., 13, 9675–9693, 2013.

2 Draxler, R.R. and Rolph, G.D. HYSPLIT (HYbrid Single-Particle Lagrangian Integrated
3 Trajectory) Model access via NOAA ARL READY Website
4 (<http://www.arl.noaa.gov/HYSPLIT.php>). NOAA Air Resources Laboratory, College Park,
5 MD.

6 Dee, D. P., Uppala, S. M., Simmons, A. J., Berrisford, P., Poli, P., Kobayashi, S., Andrae, U.,
7 Balmaseda, M. A., Balsamo, G., Bauer, P., Bechtold, P., Beljaars, A. C. M., van de Berg, L.,
8 Bidlot, J., Bormann, N., Delsol, C., Dragani, R., Fuentes, M., Geer, A. J., Haimberger, L.,
9 Healy, S. B., Hersbach, H., Hólm, E. V., Isaksen, I., Kållberg, P., Köhler, M., Matricardi, M.,
10 McNally, A. P., Monge-Sanz, B. M., Morcrette, J.-J., Park, B.-K., Peubey, C., de Rosnay, P.,
11 Tavolato, C., Thépaut, J.-N., and Vitart, F.: The ERA-Interim reanalysis: configuration and
12 performance of the data assimilation system, *Q. J. R. Meteorol. Soc.*, 137, 553–597,
13 doi:10.1002/qj.828, 2011.

14 de Laat, A. T. J., Aben, I., and Roelofs, G. J.: A model perspective on total tropospheric O₃
15 column variability and implications for satellite observations, *J. Geophys. Res.*, 110, D13303,
16 doi:10.1029/2004JD005264, 2005.

17 Dempsey, F.: Observations of stratospheric O₃ intrusions in air quality monitoring data in
18 Ontario, Canada, *Atmos. Environ.*, 98, 111–122, doi:10.1016/j.atmosenv.2014.08.024, 2014.

19 Ding, A. J., Wang, T., Thouret, V., Cammas, J.-P., and Nédélec, P.: Tropospheric ozone
20 climatology over Beijing: analysis of aircraft data from the MOZAIC program, *Atmos. Chem.*
21 *Phys.*, 8, 1-13, 2008.

22 Ding, A., Wang, T., Xue, L., Gao, J., Stohl, A., Lei, H., Jin, D., Ren, Y., Wang, X., Wei, X.,
23 Qi, Y., Liu, J., and Zhang, X.: Transport of north China air pollution by midlatitude
24 cyclones: Case study of aircraft measurements in summer 2007, *J. Geophys. Res.*, 114,
25 D08304, doi:10.1029/2008JD011023, 2009.

26 Ding, K., Liu, J., Ding, A., Liu, Q., Zhao, T. L., Shi, J., Han, Y., Wang, H., and Jiang, F.:
27 Uplifting of carbon monoxide from biomass burning and anthropogenic sources to the free
28 troposphere in East Asia, *Atmos. Chem. Phys.*, 15, 2843-2866, 2015.

29 Doche, C., Dufour, G., Foret, G., Eremenko, M., Cuesta, J., Beekmann, M., and Kalabokas,
30 P.: Summertime tropospheric ozone variability over the Mediterranean basin observed with
31 IASI, *Atmos. Chem. Phys.*, 14, 10589-10600, doi:10.5194/acp-14-10589-2014, 2014.

1 Dufour, G., Eremenko, M., Orphal, J., and Flaud, J.-M.: IASI observations of seasonal and
2 day-to-day variations of tropospheric ozone over three highly populated areas of China:
3 Beijing, Shanghai, and Hong Kong, *Atmos. Chem. Phys.*, 10, 3787-3801, 2010.

4 Dufour, G., Eremenko, M., Griesfeller, A., Barret, B., LeFlochmoën, E., Clerbaux, C., Hadji-
5 Lazaro, J., Coheur, P.-F., and Hurtmans, D.: Validation of three scientific ozone products
6 retrieved from IASI spectra using ozonesondes, *Atmos. Meas. Tech.*, 5, 611-630, 2012.

7 Edwards, D. P., Emmons, L. K., Hauglustaine, D. A., Chu, A., Gille, J. C., Kaufman, Y. J., P'etron,
8 G., Yurganov, L. N., Giglio, L., Deeter, M. N., Yudin, V., Ziskin, D. C., Warner, J., Lamarque, J.- F.,
9 Francis, G. L., Ho, S. P., Mao, D., Chan, J., and Drummond, J. R.: Observations of Carbon Monoxide
10 and Aerosol From the Terra Satellite: Northern Hemisphere Variability, *J. Geophys. Res. Atmos.*, 109,
11 D24202, doi:10.1029/2004JD004727, 2004.

12 Eremenko, M., Dufour, G., Foret, G., Keim, C., Orphal, J., Beekmann, M., Bergametti, G.,
13 and Flaud, J.-M.: Tropospheric ozone distributions over Europe during the heat wave in July
14 2007 observed from infrared nadir spectra recorded by IASI, *Geophys. Res. Lett.*, 35,
15 L18805, doi:10.1029/2008GL034803, 2008.

16 Fishman, J., Wozniak, A. E., and Creilson, J. K.: Global distribution of tropospheric ozone
17 from satellite measurements using the empirically corrected tropospheric ozone residual
18 technique: Identification of the regional aspects of air pollution, *Atmos. Chem. Phys.*, 3, 893–
19 907, 2003.

20 Foret, G., Eremenko, M., Cuesta, J., Sellitto, P., Barré, J., Gaubert, B., Coman, A., Dufour,
21 G., Liu, X., Joly, M., Doche, C., and Beekmann, M. : Ozone pollution : what can we see from
22 space ? A case study, *J. Geophys. Res. Atmos.*, 119, 8476–8499, doi:10.1002/2013JD021340,
23 2014.

24 George, M., Clerbaux, C., Hurtmans, D., Turquety, S., Coheur, P.-F., Pommier, M., Hadji-
25 Lazaro, J., Edwards, D. P., Worden, H., Luo, M., Rinsland, C., and McMillan, W.: Carbon
26 monoxide distributions from the IASI/METOP mission: evaluation with other space-borne
27 remote sensors, *Atmos. Chem. Phys.*, 9, 8317–8330, doi:10.5194/acp-9-8317-2009, 2009.

28 Hannan, J. R., Fuelberg, H. E., Crawford, J. H., Sachse, G. W., and Blake D. R. :Role of wave
29 cyclones in transporting boundary layer air to the free troposphere during the spring 2001
30 NASA/TRACE-P experiment, *J. Geophys. Res.*, 108, D20, 8782,
31 doi :10.1029/2002JD003105, 2003.

1 Hayashida, S., Liu, X., Ono, A., Yang, K., and Chance, K. : « Observations of ozone
2 enhancement in the lower troposphere over East Asia from space-borne ultraviolet
3 spectrometer, *Atmos. Chem. Phys. Discuss.*, 15, 2013-2054, 2015.

4 Holton, J. R., Haynes, P. H., McIntyre, M. E., Douglass, A. R., Rood, R. B., and Pfister, L. :
5 Stratosphere-troposphere exchange, *Rev. Geophysics*, 33, 4, 403-439, 1995.

6 Holton, J. R. : An introduction to dynamic meteorology, 4th ed., Elsevier, New York, 2004.

7 Höpfner, M., Blom, C. E., Echle, G., Glatthor, N., Hase, F., and Stiller, G.: Retrieval
8 simulations for MIPAS-STR measurements, edited by: Smith, W. L., *IRS 2000: Current
9 Problems in Atmospheric Radiation, Proc. of the Internat. Radiation Symp.*, St. Petersburg,
10 Russia, 24–29 July 2000, Hampton, Va., DEEPAK Publ., 2001.

11 Huang, J., Liu, H., Crawford, J. H., Chan, C., Considine, D. B., Zhang, Y., Zheng, X., Zhao,
12 C., Thouret, V., Oltmans, S. J., Liu, S. C., Jones, D. B. A., Steanrod, S. D., and Damon, M.
13 R. : Origin of springtime ozone enhancements in the lower troposphere over Beijing : In situ
14 measurements and model analysis, *Atmos. Chem. Phys. Discuss.*, 14, 32583-32627, 2014.

15 Hurtmans, D., Coheur, P.-F., Wespes, C., Clarisse, L., Scharf, O., Clerbaux, C., Hadji-
16 Lazaro, J., George, M., and Turquety, S. : FORLI radiative transfer and retrieval code for
17 IASI, *JQSRT*, 113, 1391-1408, doi:10.1016/j.jqsrt.2012.02.036, 2012.

18 Jaffe, D., Anderson, T., Covert, D., Kotchenruther, R., Trost, B., Danielson, J., Simpson, W.,
19 Berntsen T., Karlsdottir, S., Blake, D., Harris, J., Carmichael, G., and Uno, I. : Transport of
20 Asian air pollution to North America, *Geophys. Res. Lett.*, 26 (6), 711-714, 1999.

21 Lelieveld, J., and F. J. Dentener : What controls tropospheric ozone ?, *J. Geophys. Res.*, 105,
22 3531-3551, 2000.

23 Kulawik, S. S., Osterman, G., Jones, D. B. A., and Bowman, K.W.: Calculation of altitude-
24 dependent Tikhonov constraints for TES nadir retrievals, *IEEE T. Geosci. Remote*, 44, 1334–
25 1342, 2006.

26 Li, J., Z. Wang, H. Akimoto, C. Gao, P. Pochanart, and X. Wang (2007), Modeling study of
27 ozone seasonal cycle in lower troposphere over east Asia, *J. Geophys. Res.*, 112, D22S25,
28 doi:10.1029/2006JD008209, 2007.

29 Liang, Q., L. Jaeglé, D. A. Jaffe, P. Weiss-Penzias, A. Heckman, and J. A. Snow, Long-range
30 transport of Asian pollution to the northeast Pacific: Seasonal variations and transport

1 pathways of carbon monoxide, *J. Geophys. Res.*, 109, D23S07, doi:10.1029/2003JD004402,
2 2004.

3 Lin, M., Holloway, T., Carmichael, G. R., and Fiore, A. M. : Quantifying pollution inflow and
4 outflow over East Asia in spring with regional and global models, *Atmos. Chem. Phys.*, 10,
5 4221–4239, 2010

6 Lin, J., Pan, D., and Zhang, R.-X.: Trend and Interannual Variability of Chinese Air Pollution
7 since 2000 in Association with Socioeconomic Development: A Brief Overview, *Atmos. and*
8 *oceanic science letters*, 6, 84–89, 2013.

9 Liu, H., D. J. Jacob, I. Bey, R. M. Yantosca, B. N. Duncan, and G. W. Sachse, Transport
10 pathways for Asian pollution outflow over the Pacific: Interannual and seasonal variations, *J.*
11 *Geophys. Res.*, 108(D20), 8786, doi:10.1029/2002JD003102, 2003.

12 Liu, X., K. Chance, T.P. Kurosu, Improved ozone profile retrievals from GOME data with
13 degradation correction in reflectance, *Atmos. Chem. Phys.*, 7, 1575-1583, 2007.

14 Liu, X., P. K. Bhartia, K. Chance, R. J. D. Spurr, T. P. Kurosu, Ozone profile retrievals from
15 the Ozone Monitoring Instrument, *Atmos. Chem. Phys.*, 10, 2521-2537, 2010.

16 Liu, C. X., Liu, Y., Liu, X., and Chance, K. : Dynamical and chemical features of a cutoff low
17 over Noertheast China in July 2007 : Results from satellite measurements and reanalysis,
18 *Adv. Atmos. Sci.*, 30(2), 525-540, doi : 10.1007/s00376-012-2086-8, 2013.

19 Mari, C., M. J. Evans, P. I. Palmer, D. J. Jacob, and G. W. Sachse, Export of Asian pollution
20 during two cold front episodes of the TRACE-P experiment, *J. Geophys. Res.*, 109, D15S17,
21 doi:10.1029/2003JD004307, 2004.

22 Mauzerall, D. L., D. Narita, H. Akimoto, L. Horowitz, S. Walters, D. A. Hauglustaine, and
23 G. Brasseur: Seasonal characteristics of tropospheric ozone production and mixing ratios over
24 East Asia: A global three-dimensional chemical transport model analysis, *J. Geophys. Res.*,
25 105(D14), 17895–17910, doi:10.1029/2000JD900087, 2000.

26 McMillan, W. W., Pierce, R., Sparling, L. C., Osterman, G., McCann, K., Fischer, M. L.,
27 Rappenglueck, B., Newton, R., Turner, D. D., Kittaka, C., Evans, K., Biraud, S., Lefer, B.,
28 Andrews, A., and Oltmans, S.:An Observational and modeling strategy to investigate the
29 impact of remote sources on local air quality: A Houston, Texas case study from TEXAQS II,
30 *J. Geophys. Res. Atmos.*, 115, D01301, doi:10.1029/2009JD011973, 2010.

1 McPeters, R. D., Labow, G. J., and Logan, J. A.: Ozone climatological profiles for satellite
2 retrieval algorithms, *J. Geophys. Res.*, 112, D05308, doi:10.1029/2005JD006823, 2007.

3 Miyazaki, Y., Kondo, Y., Koike, M., Fuelberg, H. E., Kiley, C. M., Kita, K., Takegawa, N.,
4 Sachse, G. W., Flocke, F., Weinheimer, A. J., Singh, H. B., Eisele, F. L., Zondlo, M., Talbot,
5 R. W., Sandholm, S. T., Avery, M. A., and Blake, D. R. : Synoptic-scale transport of reactive
6 nitrogen over the western Pacific in spring, *J. Geophys. Res.*, 108(D20), 8788 ,
7 doi :10.1029/2002JD003248, 2003.

8 Monks, P. S.: A review of the observations and origins of the spring ozone maximum, *Atmos.*
9 *Environ.*, 34, 3545-3561, 2000.

10 Monks, P. S.: Gas-phase radical chemistry in the troposphere, *Chem. Soc. Rev.*, 34, 376–395,
11 2005.

12 Monks, P. S., Archibald, A. T., Colette, A., Cooper, O., Coyle, M., Derwent, R., Fowler, D.,
13 Granier, C., Law, K. S., Stevenson, D. S., Tarasova, O., Thouret, V., von Schneidmesser, E.,
14 Sommariva, R., Wild, O., and Williams, M. L. : Tropospheric ozone and its precursors from
15 the urban to the global scale from air quality to short-lived climate forcer, *Atmos. Chem.*
16 *Phys. Discuss.*, 14, 32709-32933, 2014.

17 Nakatani, A., Kondo, S., Hayashida, S., Nagashima, T., Sudo, K., Liu, X., Chance, K., and
18 Hirota, I. : Enhanced mid-latitude tropospheric column ozone over East Asia : Couple effects
19 of stratospheric ozone intrusion and anthropogenic sources, *J. Meteor. Soc. Japan*, 90 (2),
20 207-222, 2012.

21 Oshima, N., Koike, M., Nakamura, H., Kondo, Y., Takegawa, N., Miyazaki, Y., Blake, D. R.,
22 Shirai, T., Kita, K., Kawakami, S., and Ogawa, T. : Asian chemical outflow to the Pacific in
23 late spring observed during the PEACE-B aircraft mission, *J. Geophys. Res.*, 109, D23S05,
24 doi:10.1029/2004JD004976, 2004.

25 Richter, A., Burrows, J. P., Nub, H., Granier, C., and Niemeier, U.: Increase in tropospheric
26 nitrogen dioxide over China observed from space, *Nature*, 437, 129-132, 2005.

27 Rodgers, C. D.: Inverse methods for atmospheric sounding: Theory and practice, vol. 2,
28 World Scientific Publications, Series on Atmospheric, Ocean, Planet. Phys., Singapore, 2000.

29 Rolph, G.D. Real-time Environmental Applications and Display sYstem (READY) Website
30 (<http://www.ready.noaa.gov>). NOAA Air Resources Laboratory, College Park, MD.

1 Schuepbach, E., Davies, T. D., and Massacand, A. C. : An usual springtime ozone episode at
2 high elevation in the Swiss Alps : contributions both from cross-tropopause exchange and
3 from the boundary layer, *Atmos. Environ.*, 33, 1735-1744, 1999.

4 Safieddine, S., C. Clerbaux, M. George, J. Hadji-Lazaro, D. Hurtmans, P.-F. Coheur, C.
5 Wespes, D. Loyola, P. Valks, and N. Hao, Tropospheric ozone and nitrogen dioxide
6 measurements in urban and rural regions as seen by IASI and GOME-2, *J. Geophys. Res.*
7 *Atmos.*, 118, 10,555–10,566, doi:10.1002/jgrd.50669, 2013.

8 Seinfeld, J. H., and Pandis, S. N.: *Atmospheric Chemistry and Physics, from Air Pollution to*
9 *Climate Change*, John Wiley & Sons Inc., Toronto, Canada, 1997.

10 Stevenson, D. S., Dentener, F. J., Schultz, M. G., Ellingsen, K., van Noije, T. P. C., Wild, O.,
11 Zeng, G., Amann, M., Atherton, C. S., Bell, N., Bergmann, D. J., Bey, I., Butler, T., Cofala,
12 J., Collins, W. J., Derwent, R. G., Doherty, R. M., Drevet, J., Eskes, H. J., Fiore, A. M.,
13 Gauss, M., Hauglustaine, D. A., Horowitz, L.W., Isaksen, I. S. A., Krol, M. C., Lamarque, J.
14 F., Lawrence, M. G., Montanaro, V., Muller, J. F., Pitari, G., Prather, M. J., Pyle, J. A., Rast,
15 S., 30 Rodriguez, J. M., Sanderson, M. G., Savage, N. H., Shindell, D. T., Strahan, S. E.,
16 Sudo, K., and Szopa, S.: Multimodel ensemble simulations of present-day and near-future
17 tropospheric ozone, *J. Geophys. Res.-Atmos.*, 111, doi:10.1029/2005jd006338, 2006.

18 Stiller, G. P. (ed) with contributions from v. Clarmann, T., Dudhia, A., Echle, G., Funke, B.,
19 Glatthor, N., Hase, F., Höpfner, M., Kellmann, S., Kemnitzer, H., Kuntz, M., Linden, A.,
20 Linder, M., Stiller, G. P., and Zorn, S.: *The Karlsruhe Optimized and Precise Radiative*
21 *Transfer Algorithm (KOPRA)*, vol. FZKA 6487 of *Wissenschaftliche Berichte*,
22 *Forschungszentrum Karlsruhe, Germany*, 2000.

23 Tanimoto, H., Sawa, Y., Matsueda, H., Uno, I., Ohara, T., Yamaji, K., Kurokawa, J., and
24 Yonemura, S.: Significant latitudinal gradient in the surface ozone spring maximum over East
25 Asia, *Geophys. Res. Lett.*, 32, L21805, doi:10.1029/2005GL023514, 2005.

26 Tanimoto, H., Sawa, Y., Yonemura, S., Yumimoto, K., Matsueda, H., Uno, I., Hayasaka, T.,
27 Mukai, H., Tohjima, Y., Tsuboi, K., and Zhang, L.: Diagnosing recent CO emissions and
28 ozone evolution in East Asia using coordinated surface observations, adjoint inverse
29 modelling, and MOPITT satellite data, *Atmos. Chem. Phys*, 8, 3868-3880, 2008.

30 Tikhonov, A.: On the Solution of Incorrectly Stated Problems and a Method of
31 Regularisation, *Dokl. Acad. Nauk SSSR*, 151, 501–504, 1963.

1 Veeffkind, J. P., Aben, I., McMullan, K., Förster, H., de Vries, J., Otter, G., Claas, J., Eskes,
2 H. J., de Haan, J. F., Kleipool, Q., van Weele, M., Hasekamp, O., Hoogeveen, R., Landgraf,
3 J., Snel, R., Tol, P., Ingmann, P., Voors, R., Kruisinga, B., Vink, R., Visser, H., and Levelt, P.
4 F.: TROPOMI on the ESA Sentinel-5 Precursor: A GMES mission for global observations of
5 the atmospheric composition for climate, air quality and ozone layer applications, *Remote*
6 *Sensing of Environnement*, 120, 70-83, doi:10.1016/j.rse.2011.09.027, 2012

7 Wang, Y., Konopka, P., Liu, Y., Chen, H., Müller, R., Plöger, F., Riese, M., Cai, Z., and Lü,
8 D.: Tropospheric ozone trend over Beijing from 2002-2010: ozonesonde measurements and
9 modelling analysis, *Atmos. Chem. Phys.*, 12, 8389-8399, 2012.

10 WHO: Review of evidence on health aspects of air pollution – REVIHAAP project: final
11 technical report, WHO/Europe, 2013.

12 WMO: International list of selected and supplementary ships, 3, WMO 47 (WMO/OMM 47,
13 TP. 18), 143 pp., 1957.

14 Worden, H. M., Logan, J. A., Worden, J. R., Beer, R., Bowman, K., Clough, S. A., Eldering,
15 A., Fisher, B. M., Gunson, M. R., Herman, R. L., Kulawik, S. S., Lampel, M. C., Luo, M.,
16 Megretskaia, I. A., Osterman, G. B., and Shephard, M. W.: Comparisons of Tropospheric
17 Emission Spectrometer (TES) ozone profiles to ozonesondes: Methods and initial results, *J.*
18 *Geophys. Res.*, 112, D03309, doi:10.1029/2006JD007258, 2007.

19 Yamaji, K., Ohara, T., Uno, I., Tanimoto, H., Kurokawa, J., and Akimoto, H. : Analysis of the
20 seasonal variation of ozone in the boundary layer in East Asia using the Community Multi-
21 scale Air Quality model: What controls surface ozone levels over Japan?, *Atmos. Environ.*,
22 40, 1856–1868, 2006.

23 Zhao, C., Wang, Y., and Zeng, T.: East China plains: a “basin” of ozone pollution. *Environ.*
24 *Sci. Tech.*, 43, 1911, 2009.

25 Zhou, D. K., A. M. Larar, X. Liu, W. L. Smith, L. L. Strow, P. Yang, P. Schlüssel and X.
26 Calbet (2011), Global land surface emissivity retrieved from satellite ultraspectral IR
27 measurements, *Geosci. Rem. Sens. IEEE Trans.*, 49 (4), 1277-1290.

28

29

30 |

1
2
3
4
5
6
7
8
9
10

11 Table 1. Ozonesonde stations used for the validation. “N days” represents the number of
12 measurements matching the coincidence criteria.

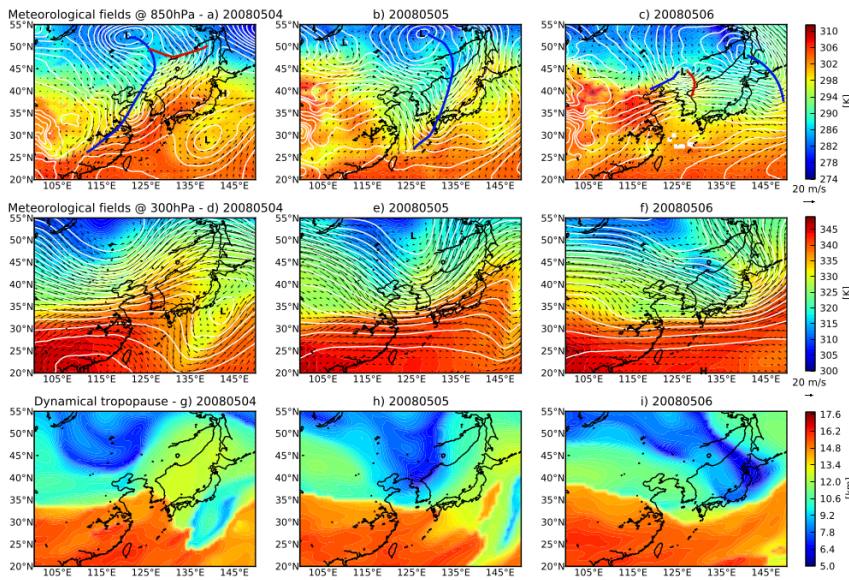
Station	Location		N days	Station	Location		N days
Ankara	39.97°N	32.86°E	50	Tateno	36.10°N	140.10°E	4
Aquila	42.38°N	13.31°E	11	Uccle	50.80°N	4.35°E	390
Barajas	40.47°N	3.58°W	139	Ushuaia	54.85°S	68.31°W	2
Beijing	39.54°N	117.12°E	7	Valentia	51.93°N	10.25°W	33
Bratts Lake	50.20°N	104.70°W	56	Wallops Island	37.90°N	75.70°W	15
Broadmeadows	37.69°S	144.94°E	19				
Churchill	58.74°N	94.07°W	46	Hanoi	21.02°N	105.80°E	16
De Bilt	52.10°N	5.18°E	104	Hilo	19.43°N	155.04°W	62
Edmonton	53.55°N	114.11°W	2	Hong Kong	22.31°N	114.17°E	93
Egbert	44.23°N	79.78°W	57	Irene	25.90°S	28.22°E	4
Goose Bay	53.31°N	60.36°W	98	Java	7.50°S	112.60°E	6
Hohenpeissenberg	47.80°N	11.00°W	319	Kuala Lumpur	2.73°N	101.70°E	5
Huntsville	34.72°N	86.64°W	9	Nairobi	1.27°S	36.80°E	78
Kelowna	49.93°N	119.40°W	124	Naha	26.20°N	127.70°E	0
Lauder	45.04°S	169.68°E	5	Natal	5.49°S	35.80°W	64
Legionowo	52.40°N	20.97°E	133	Pago	14.23°S	170.56°W	13
Lindenberg	52.21°N	14.12°E	148	Panama	7.75°N	80.25°W	2
Macquarie Island	54.50°S	158.94°E	1	Reunion	21.06°S	55.48°E	87
Payerne	46.49°N	6.57°E	389	Samoa	14.23°S	170.56°W	3
Praha	50.01°N	14.45°E	143	San Cristobal	0.92°S	89.60°W	24
Sapporo	43.10°N	141.30°E	12	Santa Cruz	28.46°N	16.26°W	2
Stony Plain	53.55°N	114.11°W	57	Watukosek	7.50°S	112.60°E	16

13

Station	Bias	RMS	R
All stations	-0.6 (2.8)	2.8 (13.7)	0.70
East Asia	-2.2 (-9.5)	2.7 (11.6)	0.70
Beijing	-2.6 (-9.0)	2.6 (9.0)	0.71

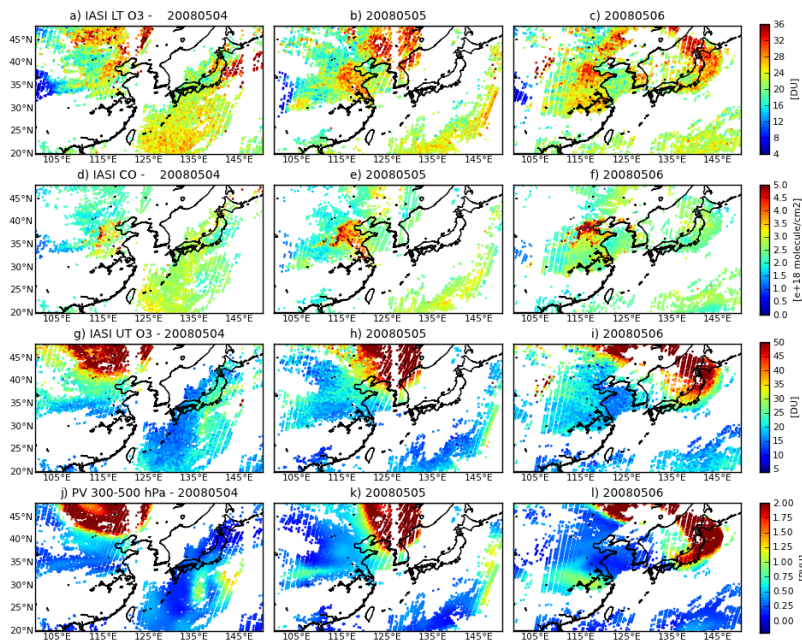
Sapporo	0.8 (3.9)	3.9 (19.8)	0.68
Tateno	-2.6 (-12.1)	2.3 (10.8)	0.60
Hong Kong	-2.6 (-10.9)	2.2 (9.6)	0.67

1
2
3
4



5

6 Figure 1. Meteorological situation given at (a-c) 850 hPa and (d-f) 300 hPa from 4 to 6 May
7 2008 as well as (g-i) the dynamical tropopause. All the meteorological variables are derived
8 from the ERA-Interim reanalysis. The color filled contours in (a-f) represent the equivalent
9 potential temperature and the white contour the geopotential height. The “L” and “H”
10 symbols represent the centre of lows and highs respectively. Horizontal winds are also
11 plotted. The cold and warm fronts are displayed in blue and red respectively on the top panel.



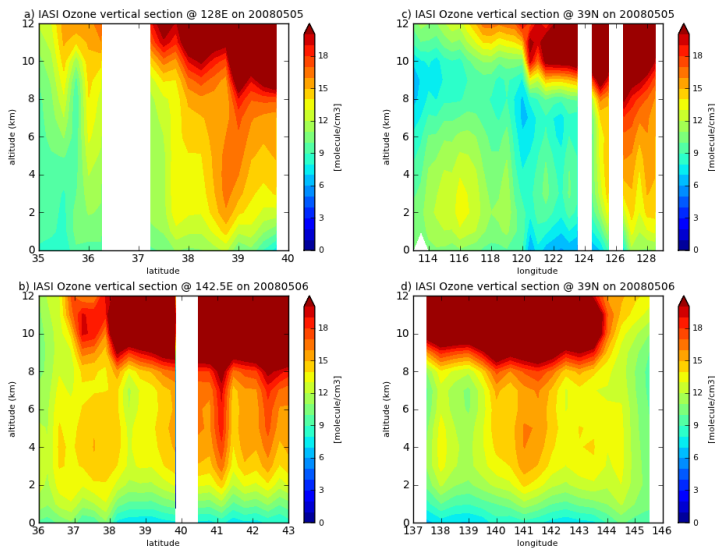
1
 2 Figure 2. (a-c) Lower-tropospheric ozone columns (surface to 6 km asl) retrieved from IASI
 3 from 4 to 6 May 2008; (d-f) Total CO columns retrieved from IASI; (g-i) Upper-tropospheric
 4 ozone columns (6 to 12 km asl) retrieved from IASI; (j-l) Potential Vorticity (PV) from ERA-
 5 Interim reanalysis averaged between 300 and 500 hPa.

Gaëlle Dufour 15/9/y 13:55

Supprimé:

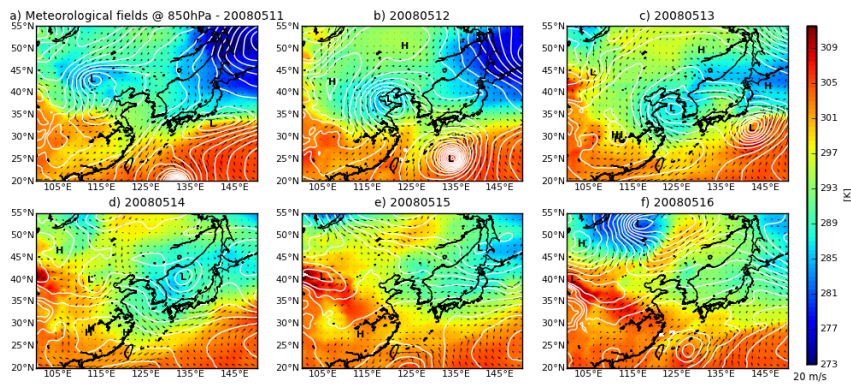
Gaëlle Dufour 15/9/y 14:05

Supprimé:



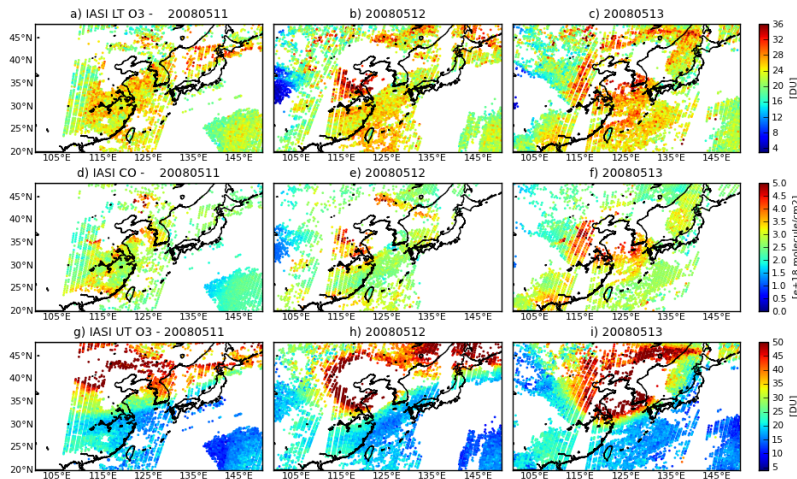
1
 2 Figure 3. Vertical section of ozone concentration (in molecule/cm³) retrieved from IASI along
 3 specific longitudes – (a) 128°E on 5 May 2008, (b) 142.5°E on 6 May 2008 – and along
 4 specific latitudes – 39°N on 5 May 2008 (c) and 6 May 2008 (d). The longitudinal
 5 (latitudinal) sections are computed over 1° around the specific longitude (latitude) with a
 6 0.25° resolution in latitude (longitude).

7
 8
 9
 10



1
2
3
4
5
6
7

Figure 4. Meteorological situation given at 850 hPa from 11 to 16 May 2008. The color filled contours represent the equivalent potential temperature and the white contour the geopotential height. The “L” and “H” symbols represent the centre of lows and highs respectively. Horizontal winds are also plotted.



8
9
10
11

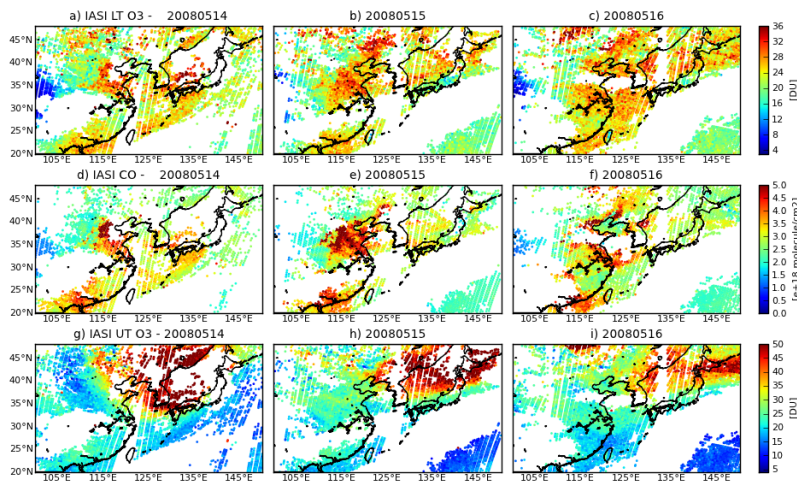
Figure 5. (a-c) Lower-tropospheric ozone columns (surface to 6 km a.s.l) retrieved from IASI from 11 to 13 May 2008. (d-f) Total CO columns retrieved from IASI. (g-i) Upper-tropospheric ozone columns (6 to 12 km a.s.l) retrieved from IASI

Gaëlle Dufour 15/9/y 13:55

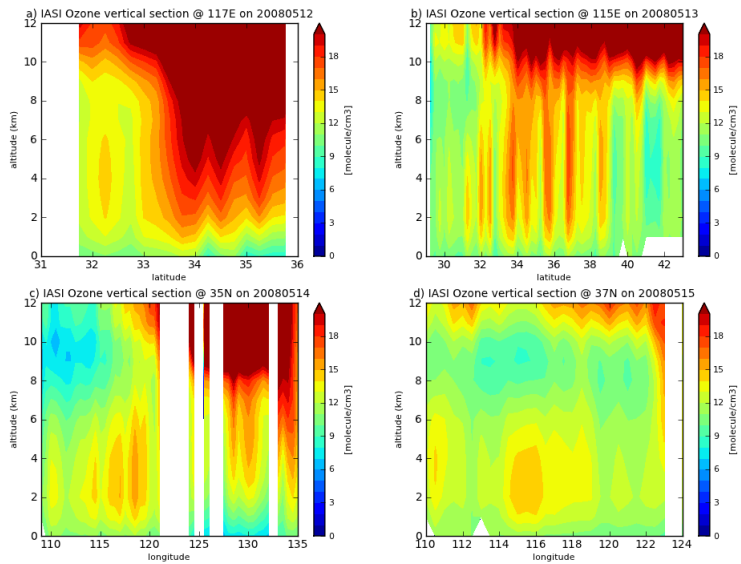
Supprimé:

Gaëlle Dufour 15/9/y 14:05

Supprimé:

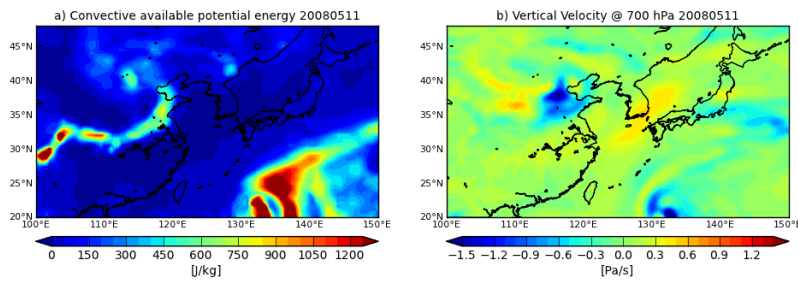


1
 2 Figure 6. Same as Fig. 6 for 14 to 16 May 2008.

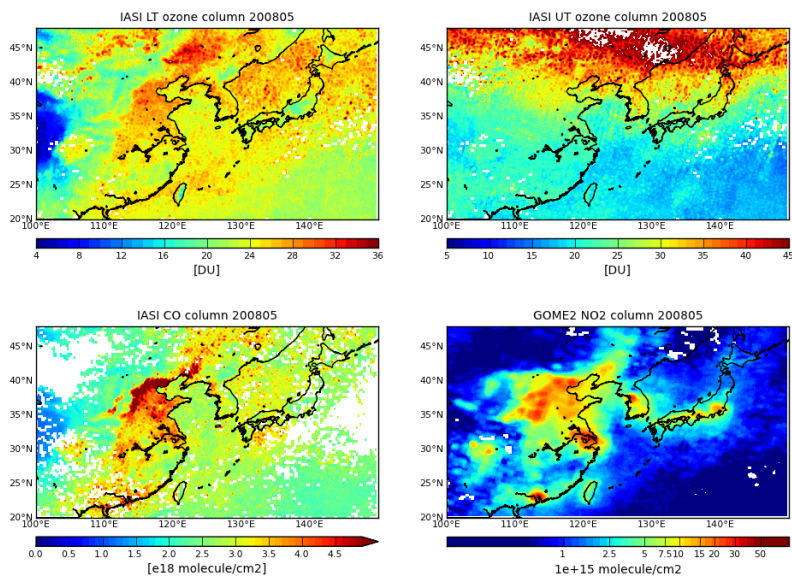


3
 4 Figure 7. Vertical section of ozone concentration (in molecule/cm³) retrieved from IASI along
 5 specific longitudes – (a) 117°E on 12 May 2008, (b) 115°E on 13 May 2008 – and along
 6 specific latitudes – (c) 35°N on 14 May 2008, (d) 37°N on 15 May 2008. The longitudinal

1 (latitudinal) sections are computed over 1° around the specific longitude (latitude) with a
2 0.25° resolution in latitude (longitude).

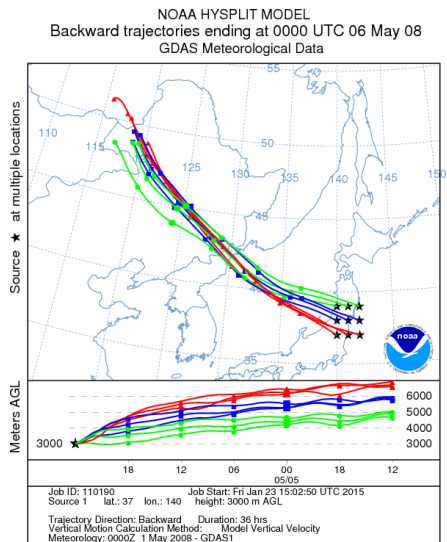


4 Figure 8. Convective available potential energy (a) and vertical velocity at 700 hPa (b) from
5 ERA-Interim reanalysis.



7 Figure 9. Monthly lower (upper left) and upper (upper right) tropospheric ozone columns
8 observed by IASI in May 2008 as well as monthly IASI total CO columns (lower left) and
9 GOME-2 NO_2 tropospheric columns (lower right) observed in May 2008. The average is
10 calculated for a $0.25^\circ \times 0.25^\circ$ resolution grid.

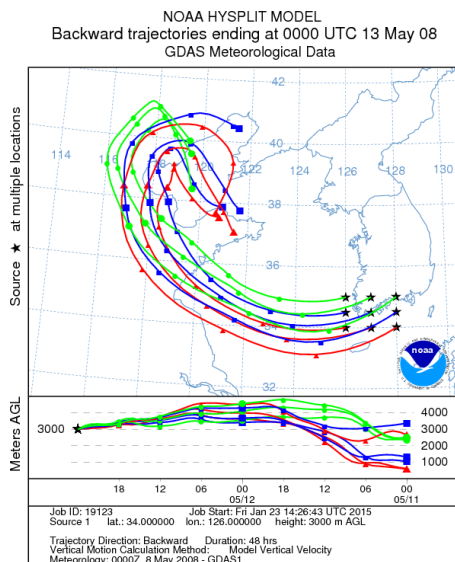
1 Supplementary material



2

3 Figure S1. 36-hours backward trajectories ending at 3km on 6 May 2008 in the region of

4 Tokyo.

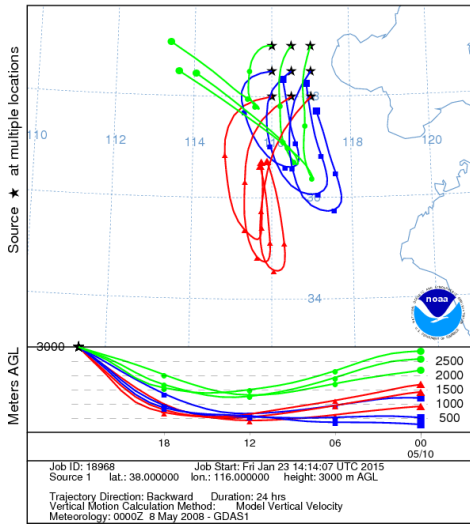


5

6 Figure S2. 48-hours backward trajectories ending at 3km on 13 May 2008 in the region of

7 South Korea.

NOAA HYSPLIT MODEL
Backward trajectories ending at 0000 UTC 11 May 08
GDAS Meteorological Data



1

2 Figure S3. 24-hours backward trajectories ending at 3km on 11 May 2008 in the region of
3 Beijing.

4